

Sensitivity-Based Model Updating for Structural Damage Identification Using Total Variation Regularization

Niklas Grip^{1*}, Natalia Sabourova^{1*, **} and Yongming Tu^{2 ††}

¹ Luleå University of Technology, SE-971 87 Luleå, Sweden, Niklas.Grip@ltu.se, Natalia.Sabourova@ltu.se.

² School of Civil Engineering, Southeast University, Nanjing, China, tuyongming@seu.edu.cn, yongming.tu@ltu.se.

Abstract

Sensitivity-based Finite Element Model Updating (FEMU) is one of the widely accepted techniques used for damage identification in structures. FEMU can be formulated as a numerical optimization problem and solved iteratively making automatic updating of the uncertain model parameters by minimizing the difference between measured and analytical structural properties. However, in the presence of noise in the measurements, the updating results are usually prone to errors. This is mathematically described as instability of the damage identification as an inverse problem. One way to resolve this problem is by using regularization. In this paper we investigate regularization methods based on the minimization of the total variation of the uncertain model parameters and compare this solution with a rather frequently used regularization based on an interpolation technique. For well-localized damages the results show a clear advantage of the proposed solution in terms of the identified location and severity of damage compared with the interpolation based solution.

For a practical test of the proposed method we use a reinforced concrete plate. Measurements and analysis were repeated first on an undamaged plate, and then after applying four different degrees of damage.

Keywords: Finite element model updating, damage identification, total variation regularization, (pseudo) Huber function, interpolation, reinforced concrete plate

1 Introduction

In this paper, we deal with finite element model updating by the classical iterative sensitivity based method [1, 2]. Compared to other finite element model updating methods, the sensitivity based method showed computational efficiency and good sensitivity to small damages [3, 2]. Basically, there are two application areas of model updating. In the first place, it is applied in order to increase the reliability of the finite element model and thus, for example, the prediction of the dynamic behavior of the structure under different loads. Another application area is damage identification in structures which is the focus of this paper.

*The authors were supported by the Swedish Research Council Formas grants (registration numbers 2007–1430 and 2012–1037) as well as by the Swedish Construction Industry’s Organisation for Research and Development (SBUF) grant 13010.

**The author was supported by Elsa and Sven Thysells Foundation for Structural Engineering Studies at Luleå University of Technology.

††The author was supported by the National Natural Science Foundation of China (project number 51378104).

In mathematical language, damage identification by finite element model updating is a parameter estimation problem. The finite element model is parameterized by uncertain parameters, which are updated by some parameter estimation technique. We assume here that the model is physically meaningful and thus can accurately represent the behavior of the actual structure, so that the damage identification problem can be reduced to the parameter estimation only. The parameter estimation problems belong to a class of inverse problems, i.e. knowing the model outputs, one need to obtain the internal model parameters. In the presence of noise in the outputs, which is the case with vibration tests, the inverse problem becomes ill-posed, i.e. small variations in the outputs lead to unreasonably large variations in the model parameters. Such problems can be solved by using regularization, which is increasingly more often consistently taken into account in the area of structural damage identification ([4, 5, 6, 7, 8, 9], etc).

In this paper, we investigate a regularization tool for the ill-posed damage identification problem that has its origin in image processing and which is associated with minimization of the total variation of the uncertain parameters. We compare then this regularization technique with a rather frequently used interpolation with so-called damage functions introduced in [8]. By using damage or interpolating functions, the algorithm is free to choose parameter values freely on a more sparse grid, and then parameters in the intermediate points are chosen by interpolation. This gives smoothing, but you lose resolution. It would be desirable to keep the highest possible resolution but add restrictions to the damage identification algorithm that favors solutions with a sharp increase of damage index close to a damage and keep damage index close to zero elsewhere. We show that the total variation regularization brings the parameter estimation close to the desirable solution and in the case of well-localized damage, it results in a more precise damage identification than the interpolation method.

In reinforced concrete structures shear cracks may form well-localized damage patterns. When such cracks develop, a brittle failure of the structure may be close — an inclined crack can find its way through a structure, without being prevented by reinforcement. It is of great interest to identify location and severity of such local cracks more precisely without smoothing the damage to the areas nearby and in this way to distinguish these cracks from other less severe cracks, such as e.g. bending cracks.

1.1 Damage parametrization

A discrete linear time-invariant model of structural motion that is central in damage identification under consideration is described by a second order differential equation:

$$M\ddot{\mathbf{u}}(t) + C\dot{\mathbf{u}}(t) + K\mathbf{u}(t) = \mathbf{f}(t), \quad (1)$$

where the matrices M , C and K are real time-independent square system mass, damping and stiffness matrices of order $d \times d$ with d corresponding to the number of degrees of freedom of the model and $\mathbf{u}(t)$ is a time dependent displacement vector with d entries. Dots represent derivatives with respect to time t and $\mathbf{f}(t)$ is a vector of external forces. Considering the free vibration case, i.e. $\mathbf{f}(t) = \mathbf{0}$ and looking for the harmonic solution of Equation (1) in the form $\mathbf{u}(t) = \boldsymbol{\phi}_k e^{j\omega_k t}$, we obtain the following generalized eigenvalue problem

$$(-\omega_k^2 M + j\omega_k C + K) \boldsymbol{\phi}_k = \mathbf{0}. \quad (2)$$

Here, $j = \sqrt{-1}$, $\lambda_k = \omega_k^2 = (2\pi f_k)^2$ and $\boldsymbol{\phi}_k$ are the k^{th} eigenvalue and eigenvector, respectively, whereas f_k is the k^{th} eigenfrequency. From Equation (2) it is easy to see that changes in system matrices M , C and K cause changes in the modal parameters λ_k and $\boldsymbol{\phi}_k$.

It is very popular to update system matrices by the substructure matrices [4, 5, 6] as follows

$$\begin{aligned} K(\boldsymbol{\alpha}) &= K^0 - \sum_{i=1}^I \alpha_i K_i, \\ M(\boldsymbol{\beta}) &= M^0 - \sum_{j=1}^J \beta_j M_j, \\ C(\boldsymbol{\gamma}) &= C^0 - \sum_{s=1}^S \gamma_s C_s, \end{aligned} \quad (3)$$

where $K(\boldsymbol{\alpha})$, $M(\boldsymbol{\beta})$ and $C(\boldsymbol{\gamma})$ are the improved matrices of the parameterized or corrected model. K_i , M_j and C_s are the constant expanded order matrices for the i^{th} , j^{th} and s^{th} element or substructure (group) representing the uncertain model property and location. α_i , β_j and γ_s are dimensionless updating parameters which can be taken as the negative relative difference of the physical parameter from its initial value, i.e. $\frac{X_t^0 - X_t}{X_t^0}$, where t is one of i , j or s . This choice of updating parameters comes naturally from the simple isotropic damage theory [10]. In this theory the damage is described by a reduction in bending stiffness, as

$$DI = \frac{E^0 - E}{E^0}, \quad (4)$$

where E^0 and E is the initial (undamaged) and updated (damaged) elasticity modulus, respectively, and DI stands for damage index. The matrices K^0 , M^0 and C^0 in (3) are interpreted as the initial analytical system matrices or matrices corresponding to the undamaged structure in the content of damage identification. The model is modified only by the updating parameters for the substructure matrices.

Thus, using the simple damage model (4) for an undamped structure whose mass does not change significantly in the degradation process, the finite element model is parameterized by

$$\begin{aligned} K(\boldsymbol{\alpha}) &= K^0 - \sum_{i=1}^I \alpha_i K_i, \text{ where } \alpha_i = \frac{E_i^0 - E_i}{E_i^0}, \\ K(\boldsymbol{\alpha})\phi_k(\boldsymbol{\alpha}) &= \lambda_k(\boldsymbol{\alpha})M\phi_k(\boldsymbol{\alpha}). \end{aligned} \quad (5)$$

Clearly, a small value of α_i , or zero in the ideal case, indicates the absence of damage for a particular element or group, positive α_i corresponds to decrease and negative α_i indicates increase of the elasticity modulus for the element or group. A good damage identification method should provide positive α_i for the elements or groups containing damages and $\alpha_i \approx 0$ for the undamaged elements of groups.

Remark. The description of damage in terms of reduction in bending stiffness only is more suitable for the simple beam structures. In the case when also torsional components of mode shapes are involved in the measurement data, it is even more advantageous to describe damage by reduction in both bending EI and torsional stiffness GI . In the later case, one can extend the finite element model parametrization by using similar type of dimensionless parameter as for the elasticity modulus, namely $\alpha_i^G = \frac{G_i^0 - G_i}{G_i^0}$, where G_i^0 and G_i are torsional shear modulus for the initial and for the updated state, respectively. Thus, the mixed elasticity and shear modulus model parametrization will be

$$K(\boldsymbol{\alpha}) = K^0 - \sum_{i=1}^I \alpha_i^E K_i^E + \alpha_i^G K_i^G, \quad (6)$$

where $\alpha_i^E = \frac{E_i^0 - E_i}{E_i^0}$, $\alpha_i^G = \frac{G_i^0 - G_i}{G_i^0}$ and K_i^E and K_i^G are the nonzero parts of the element or group constant matrix K_i connected to the degrees of freedom responsible for the bending and for the torsional stiffness, respectively.

1.2 Formulation of optimization problem

In order to solve the parameter estimation problem, we need to define so-called residual or the difference between the measured and analytical structural properties v , e.g. natural frequencies, mode shapes, frequency response functions (FRFs), etc. The residual is a function $\mathbf{r} : \mathbb{R}^n \rightarrow \mathbb{R}^m$ with n corresponding to the number of updating parameters and m equal to the number of measured observations, defined by

$$\mathbf{r}(\boldsymbol{\alpha}) = W_{\mathbf{v}}(\mathbf{v}^{mea} - \mathbf{v}(\boldsymbol{\alpha})),^a \quad (7)$$

where $W_{\mathbf{v}}$ is a weighting matrix, which is used in order to emphasize the most significant data.

One way to minimize the difference between the measured and analytical properties is to use least squares estimation. The objective function is then defined as the following weighted squared Euclidean norm of the residual vector:

$$f(\boldsymbol{\alpha}) = \frac{1}{2}(\mathbf{v}^{mea} - \mathbf{v}(\boldsymbol{\alpha}))^T W (\mathbf{v}^{mea} - \mathbf{v}(\boldsymbol{\alpha})) = \frac{1}{2} \|\mathbf{r}(\boldsymbol{\alpha})\|_2^2, \text{ with } W = W_{\mathbf{v}}^T W_{\mathbf{v}}. \quad (8)$$

Additionally, we require that some or all updating parameters are restricted by box constraints $l_i \leq \alpha_i \leq u_i$ and thus formulate a constrained nonlinear (\mathbf{r} depends nonlinearly on $\boldsymbol{\alpha}$) least squares problem as follows

$$\min_{\boldsymbol{\alpha} \in \mathbb{R}^n: l \leq \boldsymbol{\alpha} \leq u} \frac{1}{2} \|\mathbf{r}(\boldsymbol{\alpha})\|_2^2. \quad (9)$$

The nonlinear least squares problem has no closed form solution and usually is solved by iterative methods. In the presence of noise in the measured observations, the estimated parameters found by an iterative method can have a pronounced tendency to form an oscillating pattern that makes it difficult to localize and quantify the damage (see Figures 12 and 13). A standard solution of this problem is to use a regularization technique

$$\min_{\boldsymbol{\alpha} \in \mathbb{R}^n: l \leq \boldsymbol{\alpha} \leq u} \frac{1}{2} \|\mathbf{r}(\boldsymbol{\alpha})\|_2^2 + \lambda R(\boldsymbol{\alpha}), \quad (10)$$

where λ and R are the regularization parameter and the regularization function, respectively. The regularization function describes the properties of the expected solution, for example, distance from the initial guess, measure of smoothness, etc. Another type of regularization, which can be said implicitly fits the form (10) is to use the interpolation technique which was introduced in [8]. In this paper we investigate the regularization function R being described by a total variation of the parameter vector $\boldsymbol{\alpha}$.

1.2.1 Residuals and their derivatives

Let us write the vector-valued residual function $\mathbf{r} : \mathbb{R}^n \rightarrow \mathbb{R}^m$ (7) in the following form:

$$\mathbf{r}(\boldsymbol{\alpha}) = (r_1(\boldsymbol{\alpha}), r_2(\boldsymbol{\alpha}), \dots, r_m(\boldsymbol{\alpha}))^T. \quad (11)$$

^aHereafter, upper index *mea* is referring to the measured quantity. We use boldface font for vectors and $\|\cdot\|_2$ for the l_2 norm, i.e. $\|\mathbf{r}\|_2 = (|r_1|^2 + |r_2|^2 + \dots + |r_m|^2)^{1/2}$.

Each component of \mathbf{r} is a function $r_i : \mathbb{R}^n \rightarrow \mathbb{R}$. Moreover, the gradient $\nabla r(\boldsymbol{\alpha})$, the Hessian $\nabla^2 r(\boldsymbol{\alpha})$ and the Jacobian $J_r(\boldsymbol{\alpha})$ are equal to (see [11])

$$\nabla r_i(\boldsymbol{\alpha}) = \left[\frac{\partial r_i}{\partial \alpha_1} \quad \frac{\partial r_i}{\partial \alpha_2} \quad \cdots \quad \frac{\partial r_i}{\partial \alpha_n} \right]^T \in \mathbb{R}^n \quad (12)$$

$$\nabla^2 r_i(\boldsymbol{\alpha}) = \begin{bmatrix} \frac{\partial^2 r_i}{\partial \alpha_1^2} & \frac{\partial^2 r_i}{\partial \alpha_1 \partial \alpha_2} & \cdots & \frac{\partial^2 r_i}{\partial \alpha_1 \partial \alpha_n} \\ \vdots & \vdots & & \vdots \\ \frac{\partial^2 r_i}{\partial \alpha_n \partial \alpha_1} & \frac{\partial^2 r_i}{\partial \alpha_n \partial \alpha_2} & \cdots & \frac{\partial^2 r_i}{\partial \alpha_n^2} \end{bmatrix} \in \mathbb{R}^{n \times n} \quad (13)$$

$$\nabla \mathbf{r}(\boldsymbol{\alpha}) = J_r(\boldsymbol{\alpha})^T = \begin{bmatrix} \frac{\partial r_1}{\partial \alpha_1} & \frac{\partial r_2}{\partial \alpha_1} & \cdots & \frac{\partial r_m}{\partial \alpha_1} \\ \vdots & \vdots & & \vdots \\ \frac{\partial r_1}{\partial \alpha_n} & \frac{\partial r_2}{\partial \alpha_n} & \cdots & \frac{\partial r_m}{\partial \alpha_n} \end{bmatrix} = [\nabla r_1 \quad \nabla r_2 \quad \cdots \quad \nabla r_m] \in \mathbb{R}^{n \times m} \quad (14)$$

$$\nabla^2 \mathbf{r}(\boldsymbol{\alpha}) = \begin{bmatrix} \nabla \frac{\partial r_1}{\partial \alpha_1} & \nabla \frac{\partial r_2}{\partial \alpha_1} & \cdots & \nabla \frac{\partial r_m}{\partial \alpha_1} \\ \vdots & \vdots & & \vdots \\ \nabla \frac{\partial r_1}{\partial \alpha_n} & \nabla \frac{\partial r_2}{\partial \alpha_n} & \cdots & \nabla \frac{\partial r_m}{\partial \alpha_n} \end{bmatrix} = [\nabla^2 r_1 \quad \nabla^2 r_2 \quad \cdots \quad \nabla^2 r_m] \in \mathbb{R}^{n \times n \times m} \quad (15)$$

The gradient and the Hessian of $f(\boldsymbol{\alpha}) = \frac{1}{2} \|\mathbf{r}(\boldsymbol{\alpha})\|_2^2 = \frac{1}{2} \mathbf{r}(\boldsymbol{\alpha})^T \mathbf{r}(\boldsymbol{\alpha})$ are obtained by using the chain rule:

$$\nabla f(\boldsymbol{\alpha}) = \nabla \mathbf{r}(\boldsymbol{\alpha}) \mathbf{r}(\boldsymbol{\alpha}) = \sum_{j=1}^m r_j(\boldsymbol{\alpha}) \nabla r_j(\boldsymbol{\alpha}) = J_r(\boldsymbol{\alpha})^T \mathbf{r}(\boldsymbol{\alpha}) \quad (16)$$

$$\begin{aligned} \nabla^2 f(\boldsymbol{\alpha}) &= \nabla \mathbf{r}(\boldsymbol{\alpha}) \nabla \mathbf{r}(\boldsymbol{\alpha})^T + \nabla^2 \mathbf{r}(\boldsymbol{\alpha}) \mathbf{r}(\boldsymbol{\alpha}) \\ &= J_r(\boldsymbol{\alpha})^T J_r(\boldsymbol{\alpha}) + \sum_{j=1}^m r_j(\boldsymbol{\alpha}) \nabla^2 r_j(\boldsymbol{\alpha}) \approx J_r(\boldsymbol{\alpha})^T J_r(\boldsymbol{\alpha}). \end{aligned} \quad (17)$$

We notice here that what distinguishes the least squares from general optimization is that the second term in (17) for an accurate model is much less important than $J_r(\boldsymbol{\alpha})^T J_r(\boldsymbol{\alpha})$ because the residuals are small near the solution and thus the Hessian depends only on the first-order partial derivatives of the residuals. J_r is also called the sensitivity matrix and the corresponding finite element model updating is therefore often called as sensitivity based.

1.2.2 Choice of residuals

In this paper, we fit the finite element model to the data obtained by vibration tests on a reinforced concrete plate. Such experiments result in identified eigenfrequencies and mode shapes. Then, the residual is composed of two parts, the frequency residual $\mathbf{r}_f(\boldsymbol{\alpha})$ and the mode shape residual $\mathbf{r}_s(\boldsymbol{\alpha})$, by $\mathbf{r}(\boldsymbol{\alpha}) = [\mathbf{r}_f(\boldsymbol{\alpha}); \mathbf{r}_s(\boldsymbol{\alpha})]^T$.

The frequency residual $\mathbf{r}_f(\boldsymbol{\alpha})$ is typically a vector with entries ^b

$$(\mathbf{r}_f(\boldsymbol{\alpha}))_j \stackrel{\text{def}}{=} \omega(j) \frac{\lambda_j^{\text{mea}} - \lambda_j(\boldsymbol{\alpha})}{\lambda_j^{\text{mea}}}, \quad j = 1, \dots, m_f. \quad (18)$$

where the eigenvalue $\lambda_j = \omega_j^2$ and the angular frequency $\omega_j = 2\pi f_j$ correspond to the eigenfrequency f_j , m_f is the number of identified eigenfrequencies and $\omega(j)$ is the j^{th} element of the

^bThe frequency residual \mathbf{r}_f depends on the *squares* of the frequencies $f_j(\boldsymbol{\alpha})$ and f_j^{mea} . One possible motivation for this is that the corresponding period lengths $1/f$ for a mass-spring system are $1/f = 2\pi\sqrt{m/k}$, so that $(2\pi f)^2 = k/m$ is a *linear* function of the stiffness k .

diagonal of the weighting matrix $W_{\mathbf{v}}$. For the undamped eigenvalue problem (2), the eigenvalues λ_j are all real-valued and it can be assumed that the corresponding mode shapes are also real [12]. On the other hand, the measured mode shapes come from the structure with unknown damping characteristics and are usually complex. When updating the undamped finite element model the measured complex mode shapes must be approximated with real ones [5].

The division by λ_j^{mea} in (18) is done in order to obtain a similar weight for each component of the frequency residual. Moreover, it is important to ensure that the analytical and the measured mode shapes correspond to the same physical mode shape that is done by mode pairing, which is described below.

To define the mode shape residual, one needs to measure the similarity between two vectors. A popular choice in the literature on finite element model updating is the modal assurance criteria [13, 14]

$$\text{MAC}(\boldsymbol{\phi}^{\text{mea}}, \boldsymbol{\phi}) = \frac{|\langle \boldsymbol{\phi}^{\text{mea}}, \boldsymbol{\phi} \rangle|^2}{\|\boldsymbol{\phi}^{\text{mea}}\|_2^2 \|\boldsymbol{\phi}\|_2^2} = \frac{|\boldsymbol{\phi}^{\text{mea}H} \boldsymbol{\phi}|^2}{\|\boldsymbol{\phi}^{\text{mea}}\|_2^2 \|\boldsymbol{\phi}\|_2^2}, \quad (19)$$

where $\langle \cdot, \cdot \rangle$ denotes the scalar product and \mathbf{v}^H is the Hermitian (complex conjugate transpose) of vector \mathbf{v} . From the discussion above, it can be assumed that both the analytical and the measured mode shapes are real and thus the Hermitian can be substituted with the transpose operator. MAC measures the difference between two vectors in terms of their collinearity and not magnitudes. Using the MAC function one can pair analytical and measured mode shapes. For the paired mode shapes, one can then scale the mode shape $\boldsymbol{\phi}^{\text{mea}}$ to the magnitude (norm) and "orientation" of the analytical mode shape $\boldsymbol{\phi}$ by $MSF(\boldsymbol{\phi}^{\text{mea}}, \boldsymbol{\phi})\boldsymbol{\phi}^{\text{mea}}$ using so-called modal scale factor

$$MSF(\boldsymbol{\phi}^{\text{mea}}, \boldsymbol{\phi}) = \frac{\langle \boldsymbol{\phi}^{\text{mea}}, \boldsymbol{\phi} \rangle}{\|\boldsymbol{\phi}^{\text{mea}}\|_2^2}. \quad (20)$$

Then, the relation between norms can be checked by using the Cauchy-Schwarz inequality

$$\left\| \frac{\langle \boldsymbol{\phi}^{\text{mea}}, \boldsymbol{\phi} \rangle}{\|\boldsymbol{\phi}^{\text{mea}}\|_2^2} \boldsymbol{\phi}^{\text{mea}} \right\| \leq \frac{\|\boldsymbol{\phi}^{\text{mea}}\|_2 \|\boldsymbol{\phi}\|_2}{\|\boldsymbol{\phi}^{\text{mea}}\|_2} \frac{\|\boldsymbol{\phi}^{\text{mea}}\|_2}{\|\boldsymbol{\phi}^{\text{mea}}\|_2} \leq \|\boldsymbol{\phi}\|_2.$$

Equality holds when $\boldsymbol{\phi}^{\text{mea}}$ and $\boldsymbol{\phi}$ are collinear. To define the mode shape residual one can, for example, use the following formula

$$(\mathbf{r}_s(\boldsymbol{\alpha}))_{j,k} \stackrel{\text{def}}{=} \omega(m_f + (j-1)d + k) \left(\frac{\boldsymbol{\phi}_j^{\text{mea}T} \boldsymbol{\phi}_j(\boldsymbol{\alpha})}{\|\boldsymbol{\phi}_j^{\text{mea}}\|_2^2} \phi_{j,k}^{\text{mea}} - \phi_{j,k}(\boldsymbol{\alpha}) \right), \quad j = 1, \dots, m_f, \quad k = 1, \dots, d \quad (21)$$

to compose $\mathbf{r}_s = [r_{s_1} \ r_{s_2} \ \dots \ r_{s_{m_f \times d}}]^T$, where the ω term is the $(m_f + (j-1)d + k)^{\text{th}}$ element of the diagonal of the weighting matrix $W_{\mathbf{v}}$ (see Equation (7)), for which the first m_f elements are reserved to the weights of the eigenfrequencies.

Then, the sensitivity matrix $J_{\mathbf{r}}$ is obtained using

$$\frac{\partial r_{f_j}}{\partial \alpha_i} = \omega(j) \frac{1}{\lambda_j^{\text{mea}}} \frac{\partial \lambda_j}{\partial \alpha_i} \quad (22a)$$

$$\frac{\partial r_{s_{j,k}}}{\partial \alpha_i} = \omega(m_f + (j-1)d + k) \left(\frac{\boldsymbol{\phi}_j^{\text{mea}T} \frac{\partial \boldsymbol{\phi}_j}{\partial \alpha_i}}{\|\boldsymbol{\phi}_j^{\text{mea}}\|_2^2} \phi_{j,k}^{\text{mea}} - \frac{\partial \phi_{j,k}}{\partial \alpha_i} \right) \quad (22b)$$

The derivatives of modal data with respect to the updating parameters are computed using the Fox-Kapoor formulas [15]. In the case of the finite element model parametrization (5) these

formulas are simplified to

$$\frac{\partial \lambda_j}{\partial \alpha_i} = \phi_j^\top \frac{\partial K}{\partial \alpha_i} \phi_j = -\phi_j^\top K_i \phi_j \quad (23a)$$

$$\frac{\partial \phi_j}{\partial \alpha_i} = \sum_{q \neq j} \frac{\phi_i^\top \frac{\partial K}{\partial \alpha_i} \phi_j}{\lambda_j - \lambda_q} \phi_q = \sum_{q \neq j} \frac{\phi_i^\top K_i \phi_j}{\lambda_q - \lambda_j} \phi_q \quad (23b)$$

The number of modes in (23b) should be big enough to contribute to well-conditioning of the sensitivity matrix J_r .

1.2.3 Problem solution

In order to solve the optimization problem (10) we use the "built-in" Matlab function `fmincon` [16], which we supply with the objective function value, its gradient and Hessian on each iteration step. For the nonregularized problem (9), the required formulas are (8), (16) and (17), the residuals are computed by (18) and (21) and their derivatives are found by (22) and (23). When the regularization is involved, these formulas will be modified as it is explained in the next section.

2 Problem regularization

We use the notion of total variation of parameters to define the regularization function in Equation (10). The total variation is then supplied with l_2 -norm and combination of l_1 and l_2 -norms. In general, the l_1 -norm total variation regularization results in a piecewise constant parameter estimation which keeps sharp jumps in the parameters in the solution if they are presented and smooths out slowly varying parameters. On the other hand the l_2 -norm total variation regularization not only smooths out the slowly varying parameters but also smooths out the sharp variations [17, 18, 19].

2.1 Total variation

Assume first that the parameter vector α is distributed over a 2D grid as follows

$$A = \begin{bmatrix} \alpha_1 & \alpha_{d_1+1} & \cdots & \alpha_{(d_2-1)d_1+1} \\ \alpha_2 & \alpha_{d_1+2} & \cdots & \alpha_{(d_2-1)d_1+2} \\ \vdots & \vdots & \ddots & \vdots \\ \alpha_{d_1} & \alpha_{2d_1} & \cdots & \alpha_n \end{bmatrix} \in \mathbb{R}^{d_1 \times d_2} \quad (24)$$

with $d_1 d_2 = n$, where n is the number of updating parameters. Let us define the isotropic (invariant under rotations) total variation of a matrix A . Denote an element of this matrix at row i and column j by $A_{i,j}$ and define the operators

$$D_{h_{i,j}A} = \begin{cases} A_{i+1,j} - A_{i,j}, & \text{if } i < d_1 \\ 0, & \text{if } i = d_1 \end{cases} \quad D_{v_{i,j}A} = \begin{cases} A_{i,j+1} - A_{i,j}, & \text{if } j < d_2 \\ 0, & \text{if } j = d_2 \end{cases}.$$

Compose a "discrete gradient" of A by

$$D_{i,jA} = \begin{bmatrix} D_{h_{i,j}A} \\ D_{v_{i,j}A} \end{bmatrix},$$

where h stands for differences between horizontal rows and v stands for differences between vertical columns of the matrix A . Then, the isotropic total variation of A is given by

$$Var_1(A) = \sum_{ij} \sqrt{D_{h;ijA}^2 + D_{v;ijA}^2} = \sum_{ij} \|D_{i,jA}\|_2. \quad (25)$$

Now one can consider the regularized problem (10) with $R(\boldsymbol{\alpha}) = Var_1(A)$ or l_1 -norm total variation regularization. Note that if A is just a row or a column vector, i.e. $A = \boldsymbol{\alpha}$, then $Var_1(A)$ is reduced to $\sum_j |D_{1,jA}|$ or $\sum_i |D_{i,1A}|$, respectively. Unfortunately, the function $Var_1(A)$ is not differentiable. To resolve this problem for the methods which require first order derivatives the total variation is usually modified in the following way:

$$Var_\varphi(A) = \sum_{ij} \varphi(\|D_{i,jA}\|_2). \quad (26)$$

The straightforward choice of φ in Equation (26) is $\varphi(x) = x^2$ and thus the l_2 -norm total variation regularization with $R(\boldsymbol{\alpha})$ in (10) equals to

$$Var_2(A) = \sum_{ij} D_{h;ijA}^2 + D_{v;ijA}^2. \quad (27)$$

However, introducing the l_2 -norm for differentiability leads to an overregularized solution that destroys the effect of edges [17, 20] and therefore is not a good choice in cases when more precise damage localization is required. Another choice of φ that resembles more the behavior of the absolute value function is a differentiable so-called Huber function φ_μ^H ([21], Section 4, point (iii))

$$\varphi_\mu^H(x) = \begin{cases} x^2/(2\mu), & \text{if } |x| \leq \mu \\ |x| - \mu/2, & \text{if } |x| \geq \mu \end{cases}. \quad (28)$$

Such defined Huber function is a smooth approximation of the absolute value function. The smaller the parameter μ the better the approximation of the absolute value function. Then, the corresponding Huber total variation is

$$Var_H(A) = \sum_{ij} \varphi_\mu^H(\|D_{i,jA}\|_2). \quad (29)$$

Unfortunately, the Huber function is only first-order differentiable. Further improvement of the total variation for the second-order methods usually leads to the so-called pseudo Huber function [22], which is defined by

$$\varphi_\mu^{PH}(x) = \mu(\sqrt{1 + (x/\mu)^2} - 1). \quad (30)$$

The pseudo Huber total variation is given by

$$Var_{PH}(A) = \sum_{ij} \phi_\mu^{PH}\left(\sqrt{D_{h;ijA}^2 + D_{v;ijA}^2}\right) = \sum_{ij} \varphi_\mu^{PH}(\|D_{i,jA}\|_2). \quad (31)$$

For small values of x , the function φ_μ^{PH} approximates x^2/μ (use Taylor series expansion). For large values of x it tends to $|x|$. It has derivatives of any order. Figure 1 shows the difference between the Huber, pseudo Huber, absolute value and quadratic functions for $\mu = 0.1$.

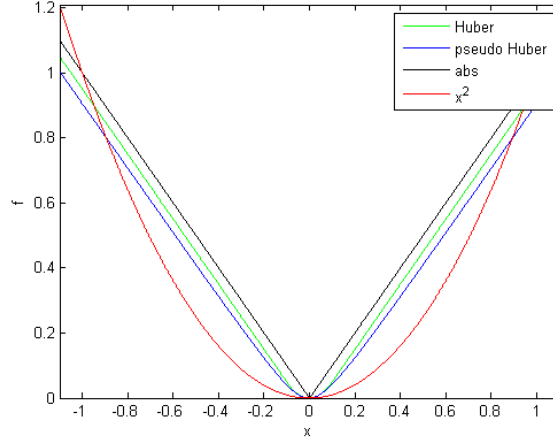


Figure 1: Comparison of Huber, pseudo Huber, absolute value and quadratic functions for $\mu = 0.1$.

2.2 l_2 norm total variation regularization

Taking $\varphi(x) = x^2$ in Equation (26), we can view the problem (10) as a penalized least squares problem with regularization applied directly to problem (9) as follows

$$\min_{\alpha \in \mathbb{R}^n: l \leq \alpha \leq u} \frac{1}{2} \|\mathbf{r}(\alpha)\|_2^2 + \lambda \text{Var}_2(A), \quad (32)$$

where $\text{Var}_2(A)$ is defined by Equation (27) and A is connected to α by Equation (24). We show now how to modify the residual vector and its Jacobian for Problem (9) so that the solution suggested in Section 1.2.3 can be used for the optimization problem (32).

Define the Toeplitz matrix $D(n)$ by

$$D(n) = \begin{bmatrix} -1 & 1 & 0 & \cdots & 0 \\ 0 & -1 & 1 & \ddots & \vdots \\ \vdots & \ddots & \ddots & \ddots & 0 \\ 0 & \cdots & 0 & -1 & 1 \end{bmatrix} \in \mathbb{R}^{(n-1) \times n}. \quad (33)$$

Define $D_v = AD(d_2)^T$ and $D_h = D(d_1)A$. Then, D_v is a $d_1 \times (d_2 - 1)$ matrix with elements $D_{v_{i,j}A}$ and D_h is a $(d_1 - 1) \times d_2$ matrix with elements $D_{h_{i,j}A}$. Taking the elements of the matrices D_v and D_h columnwise, we build two residual vectors \mathbf{r}_v and \mathbf{r}_h , respectively. It is easy to check that for $d_2 > 1$

$$\mathbf{r}_v = \begin{bmatrix} \alpha_{1+d_1} - \alpha_1 \\ \alpha_{2+d_1} - \alpha_2 \\ \cdots \\ \alpha_n - \alpha_{(d_2-1)d_1} \end{bmatrix} = \begin{bmatrix} -1 & \overbrace{0 \cdots 0}^{d_1-1} & 1 & 0 & \cdots & 0 \\ 0 & -1 & 0 & \ddots & 0 & 1 & \ddots & \vdots \\ \vdots & \ddots & \ddots & \ddots & \ddots & \ddots & \ddots & 0 \\ 0 & \cdots & 0 & -1 & 0 & \cdots & 0 & 1 \end{bmatrix} \begin{bmatrix} \alpha_1 \\ \alpha_2 \\ \cdots \\ \alpha_n \end{bmatrix} = J_v \alpha$$

and for $d_1 > 1$

$$\mathbf{r}_h = \begin{bmatrix} \alpha_2 - \alpha_1 \\ \dots \\ \alpha_{d_1} - \alpha_{d_1-1} \\ \alpha_{d_1+2} - \alpha_{d_1+1} \\ \dots \\ \alpha_{2d_1} - \alpha_{2d_1-1} \\ \dots \\ \alpha_{(d_2-1)d_1+2} - \alpha_{(d_2-1)d_1+1} \\ \dots \\ \alpha_n - \alpha_{n-1} \end{bmatrix} = \begin{bmatrix} D(d_1) & & & 0 \\ & D(d_1) & & \\ & & \ddots & \\ 0 & & & D(d_1) \end{bmatrix} \begin{bmatrix} \alpha_1 \\ \alpha_2 \\ \dots \\ \alpha_n \end{bmatrix} = J_h \boldsymbol{\alpha},$$

where J_h has d_2 blocks $D(d_1)$ on the diagonal. Then, the expanded residual and the Jacobian for the problem (32) are

$$\mathbf{r} = \begin{bmatrix} \mathbf{r} \\ \sqrt{2\lambda} J_v \boldsymbol{\alpha} \\ \sqrt{2\lambda} J_h \boldsymbol{\alpha} \end{bmatrix} \quad \text{and} \quad J_r = \begin{bmatrix} J_r \\ \sqrt{2\lambda} J_v \\ \sqrt{2\lambda} J_h \end{bmatrix}.$$

For the 1D problem, when for example, $d_1 = 1$, the matrix D_h is not defined and neither are \mathbf{r}_h or J_h . On the other hand, $J_v = D(d_2)$ and $\mathbf{r}_v = D(d_2)p$. Thus,

$$\mathbf{r} = \begin{bmatrix} \mathbf{r} \\ \sqrt{2\lambda} D(d_2) \boldsymbol{\alpha} \end{bmatrix} \quad J_r = \begin{bmatrix} J_r \\ \sqrt{2\lambda} D(d_2) \end{bmatrix}.$$

For Matlab code computing the updated \mathbf{r} and J_r , see the function `l2tv` in Appendix A.

2.3 Huber total variation regularization

For Equation (26) with $\varphi(x) = \varphi_\mu^H(x)$ defined in (28), we get from (10) the regularization problem

$$\min_{\boldsymbol{\alpha} \in \mathbb{R}^n: \mathbf{l} \leq \boldsymbol{\alpha} \leq \mathbf{u}} \frac{1}{2} \|\mathbf{r}(\boldsymbol{\alpha})\|_2^2 + \lambda \text{Var}_H(A) = \min_{\boldsymbol{\alpha} \in \mathbb{R}^n: \mathbf{l} \leq \boldsymbol{\alpha} \leq \mathbf{u}} F(\boldsymbol{\alpha}), \quad (34)$$

where $\text{Var}_H(A)$ is defined by Equation (29) and A is connected to $\boldsymbol{\alpha}$ by Equation (24). This is not a least squares problem.

In order to compute the gradient $\nabla \text{Var}_H(\boldsymbol{\alpha})$ and the Hessian $\nabla^2 \text{Var}_H(\boldsymbol{\alpha})$, we need the first and second order derivatives of φ_μ^H with respect to the parameters $A_{i,j}$ and therefore α_k . For $(\varphi_\mu^H)_{ij} = \varphi_\mu^H(\|D_{ijA}\|)$, we get

$$\frac{\partial(\varphi_\mu^H)_{ij}}{\partial A_{i,j}} = \begin{cases} -\frac{D_{h_{i,j}A} + D_{v_{i,j}A}}{\|D_{i,jA}\|_2} & \|D_{i,jA}\|_2 \leq \mu \\ -\frac{D_{h_{i,j}A} + D_{v_{i,j}A}}{\|D_{i,jA}\|_2} & \|D_{i,jA}\|_2 \geq \mu \end{cases} \quad (35)$$

$$\frac{\partial(\varphi_\mu^H)_{i-1,j}}{\partial A_{i,j}} = \begin{cases} \frac{D_{h_{i-1,j}}}{\mu} & \|D_{i-1,jA}\|_2 \leq \mu \\ \frac{D_{h_{i-1,j}A}}{\|D_{i-1,jA}\|_2} & \|D_{i-1,jA}\|_2 \geq \mu \end{cases} \quad (36)$$

$$\frac{\partial(\varphi_\mu^H)_{i,j-1}}{\partial A_{i,j}} = \begin{cases} \frac{D_{v_{i,j-1}A}}{\mu} & \|D_{i,j-1A}\|_2 \leq \mu \\ \frac{D_{v_{i,j-1}A}}{\|D_{i,j-1A}\|_2} & \|D_{i,j-1A}\|_2 \geq \mu \end{cases} \quad (37)$$

The nonzero second-order derivatives are the following

$$\frac{\partial^2(\varphi_\mu^H)_{ij}}{\partial A_{i,j}^2} = \begin{cases} \frac{2}{\mu} & \|D_{i,jA}\|_2 \leq \mu \\ \frac{(D_{h_{i,j}A} - D_{v_{i,j}A})^2}{\|D_{i,jA}\|_2^3} & \|D_{i,jA}\|_2 > \mu \end{cases} \quad (38)$$

$$\frac{\partial^2(\varphi_\mu^H)_{i-1,j}}{\partial A_{i,j}^2} = \begin{cases} \frac{1}{\mu} & \|D_{i-1,jA}\|_2 \leq \mu \\ \frac{D_{v_{i-1,j}A}^2}{\|D_{i-1,jA}\|_2^3} & \|D_{i-1,jA}\|_2 > \mu \end{cases} \quad (39)$$

$$\frac{\partial^2(\varphi_\mu^H)_{i,j-1}}{\partial A_{i,j}^2} = \begin{cases} \frac{1}{\mu} & \|D_{i,j-1A}\|_2 \leq \mu \\ \frac{D_{h_{i,j-1}A}^2}{\|D_{i,j-1A}\|_2^3} & \|D_{i,j-1A}\|_2 > \mu \end{cases} \quad (40)$$

$$\frac{\partial^2(\varphi_\mu^H)_{ij}}{\partial A_{i+1,j} \partial A_{i,j}} = \begin{cases} -\frac{1}{\mu} & \|D_{i,jA}\|_2 \leq \mu \\ \frac{D_{v_{i,j}A}(D_{h_{i,j}A} - D_{v_{i,j}A})}{\|D_{i,jA}\|_2^3} & \|D_{i,jA}\|_2 > \mu \end{cases} \quad (41)$$

$$\frac{\partial^2(\varphi_\mu^H)_{i-1,j}}{\partial A_{i-1,j} \partial A_{i,j}} = \begin{cases} -\frac{1}{\mu} & \|D_{i-1,jA}\|_2 \leq \mu \\ \frac{D_{v_{i-1,j}A}(D_{h_{i-1,j}A} - D_{v_{i-1,j}A})}{\|D_{i-1,jA}\|_2^3} & \|D_{i-1,jA}\|_2 > \mu \end{cases} \quad (42)$$

$$\frac{\partial^2(\varphi_\mu^H)_{ij}}{\partial A_{i,j+1} \partial A_{i,j}} = \begin{cases} -\frac{1}{\mu} & \|D_{i,jA}\|_2 \leq \mu \\ \frac{D_{h_{i,j}A}(D_{v_{i,j}A} - D_{h_{i,j}A})}{\|D_{i,jA}\|_2^3} & \|D_{i,jA}\|_2 > \mu \end{cases} \quad (43)$$

$$\frac{\partial^2(\varphi_\mu^H)_{i,j-1}}{\partial A_{i,j-1} \partial A_{i,j}} = \begin{cases} -\frac{1}{\mu} & \|D_{i,j-1A}\|_2 \leq \mu \\ \frac{D_{h_{i,j-1}A}(D_{v_{i,j-1}A} - D_{h_{i,j-1}A})}{\|D_{i,j-1A}\|_2^3} & \|D_{i,j-1A}\|_2 > \mu \end{cases} \quad (44)$$

$$\frac{\partial^2(\varphi_\mu^H)_{i-1,j}}{\partial A_{i-1,j+1} \partial A_{i,j}} = \begin{cases} 0 & \|D_{i-1,jA}\|_2 \leq \mu \\ -\frac{D_{h_{i-1,j}A} D_{v_{i-1,j}A}}{\|D_{i-1,jA}\|_2^3} & \|D_{i-1,jA}\|_2 > \mu \end{cases} \quad (45)$$

$$\frac{\partial^2(\varphi_\mu^H)_{i,j-1}}{\partial A_{i+1,j-1} \partial A_{i,j}} = \begin{cases} 0 & \|D_{i,j-1A}\|_2 \leq \mu \\ -\frac{D_{h_{i,j-1}A} D_{v_{i,j-1}A}}{\|D_{i,j-1A}\|_2^3} & \|D_{i,j-1A}\|_2 > \mu \end{cases} \quad (46)$$

Then, the gradient $\nabla Var_H(\boldsymbol{\alpha})$ can be found by using Equations (35)–(37) as follows

$$\nabla Var_H(\boldsymbol{\alpha})_{(j-1)d_1+i} \stackrel{\text{def}}{=} \frac{\partial Var_H(\boldsymbol{\alpha})}{\partial \alpha_{(j-1)d_1+i}} = \begin{cases} \frac{\partial(\varphi_\mu^H)_{ij}}{\partial A_{i,j}} & i = 1, j = 1 \\ \frac{\partial(\varphi_\mu^H)_{ij}}{\partial A_{i,j}} + \frac{\partial(\varphi_\mu^H)_{i-1,j}}{\partial A_{i,j}} & 2 \leq i \leq d_1, j = 1 \\ \frac{\partial(\varphi_\mu^H)_{ij}}{\partial A_{i,j}} + \frac{\partial(\varphi_\mu^H)_{i,j-1}}{\partial A_{i,j}} & i = 1, 2 \leq j \leq d_2 \\ \frac{\partial(\varphi_\mu^H)_{ij}}{\partial A_{i,j}} + \frac{\partial(\varphi_\mu^H)_{i-1,j}}{\partial A_{i,j}} + \frac{\partial(\varphi_\mu^H)_{i,j-1}}{\partial A_{i,j}} & 2 \leq i \leq d_1, 2 \leq j \leq d_2 \end{cases}.$$

The Hessian $\nabla^2 Var_H(\boldsymbol{\alpha})$ is a $(d_1 d_2) \times (d_1 d_2)$ symmetric matrix. So one can compute its upper triangular part $(\nabla^2 Var_H(\boldsymbol{\alpha}))^U$ and then expand it to the symmetric matrix. Equations (38)–(40) correspond to the elements on the main diagonal of the Hessian matrix. Equation (41) is connected to the diagonal $[k, k + 1]$, Equation (43) to the diagonal $[k, k + d_1]$ and Equation (45) to the diagonal $[k, k + d_1 - 1]$. Note, that Equations (42), (44) and (46) correspond to the lower triangular part of the Hessian and thus are already considered by Equations (41), (43)

and (45), respectively. Thus,

$$\begin{aligned}
(\nabla^2 Var_H(\boldsymbol{\alpha}))_{k_1, k_2}^U &\stackrel{\text{def}}{=} \frac{\partial^2 Var_H(\boldsymbol{\alpha})}{\partial \alpha_{k_2} \partial \alpha_{k_1}} \\
&= \begin{cases} \frac{\partial^2 (\varphi_\mu^H)_{11}}{\partial A_{1,1}^2} & k_1 = k_2 = 1 \\ \frac{\partial^2 (\varphi_\mu^H)_{i1}}{\partial A_{i,1}^2} + \frac{\partial^2 (\varphi_\mu^H)_{i-1,1}}{\partial A_{i,1}^2} & k_1 = k_2 = i, 2 \leq i \leq d_1 \\ \frac{\partial^2 (\varphi_\mu^H)_{1j}}{\partial A_{1,j}^2} + \frac{\partial^2 (\varphi_\mu^H)_{1,j-1}}{\partial A_{1,j}^2} & k_1 = k_2 = (j-1)d_1 + 1, \\ & 2 \leq j \leq d_2 \\ \frac{\partial^2 (\varphi_\mu^H)_{ij}}{\partial A_{i,j}^2} + \frac{\partial^2 (\varphi_\mu^H)_{i-1,j}}{\partial A_{i,j}^2} + \frac{\partial^2 (\varphi_\mu^H)_{i,j-1}}{\partial A_{i,j}^2} & k_1 = k_2 = (j-1)d_1 + i, \\ & 2 \leq i \leq d_1, 2 \leq j \leq d_2 \\ \frac{\partial^2 (\varphi_\mu^H)_{ij}}{\partial A_{i+1,j} \partial A_{i,j}} & k_1 = (j-1)d_1 + i, k_2 = k_1 + 1, \\ & 1 \leq i \leq d_1 - 1, 1 \leq j \leq d_2 \\ \frac{\partial^2 (\varphi_\mu^H)_{ij}}{\partial A_{i,j+1} \partial A_{i,j}} & k_1 = (j-1)d_1 + i, k_2 = k_1 + d_1, \\ & 1 \leq i \leq d_1, 1 \leq j \leq d_2 - 1 \\ \frac{\partial^2 (\varphi_\mu^H)_{i-1,j}}{\partial A_{i-1,j+1} \partial A_{i,j}} & k_1 = (j-1)d_1 + i, k_2 = k_1 + d_1 - 1, \\ & 2 \leq i \leq d_1, 1 \leq j \leq d_2 - 1 \\ 0 & \text{otherwise} \end{cases}
\end{aligned}$$

Then, for the objective function F defined by Equation (34) we have

$$\begin{aligned}
F(\boldsymbol{\alpha}) &= f(\boldsymbol{\alpha}) + \lambda Var_H(\boldsymbol{\alpha}), \\
\nabla F(\boldsymbol{\alpha}) &= \nabla f(\boldsymbol{\alpha}) + \lambda \nabla Var_H(\boldsymbol{\alpha}), \\
\nabla^2 F(\boldsymbol{\alpha}) &= \nabla^2 f(\boldsymbol{\alpha}) + \lambda \nabla^2 Var_H(\boldsymbol{\alpha}),
\end{aligned}$$

where $f(\boldsymbol{\alpha})$, $\nabla f(\boldsymbol{\alpha})$ and $\nabla^2 f(\boldsymbol{\alpha})$ are defined in Equations (8), (18), (21), (16) and (17).

For Matlab code computing $Var_H(\boldsymbol{\alpha})$, $\nabla Var_H(\boldsymbol{\alpha})$ and $\nabla^2 Var_H(\boldsymbol{\alpha})$, see the function *htv* in Appendix A.

2.4 Pseudo Huber total variation regularization

Equation (26) with $\varphi(x) = \varphi_\mu^{PH}(x)$ defined in (30) gives the regularization problem

$$\min_{\boldsymbol{\alpha} \in \mathbb{R}^n: \mathbf{l} \leq \boldsymbol{\alpha} \leq \mathbf{u}} \frac{1}{2} \|\mathbf{r}(\boldsymbol{\alpha})\|_2^2 + \lambda Var_{PH}(A) = \min_{\boldsymbol{\alpha} \in \mathbb{R}^n: \mathbf{l} \leq \boldsymbol{\alpha} \leq \mathbf{u}} F(\boldsymbol{\alpha}), \quad (47)$$

where $Var_{PH}(A)$ is defined by Equation (31) and A is connected to $\boldsymbol{\alpha}$ by Equation (24). It is not a least squares problem. The following expressions can be used in order to find $\nabla Var_{PH}(\boldsymbol{\alpha})$ and $\nabla^2 Var_{PH}(\boldsymbol{\alpha})$

$$\begin{aligned}
\frac{\partial (\varphi_\mu^{PH})_{ij}}{\partial A_{i,j}} &= -\frac{1}{\mu} \frac{D_{h_{i,j}A} + D_{v_{i,j}A}}{\sqrt{1 + \|D_{i,j}A\|_2^2 / \mu^2}} \\
\frac{\partial (\varphi_\mu^{PH})_{i-1,j}}{\partial A_{i,j}} &= \frac{1}{\mu} \frac{D_{h_{i-1,j}A}}{\sqrt{1 + \|D_{i-1,j}A\|_2^2 / \mu^2}} \\
\frac{\partial (\varphi_\mu^{PH})_{i,j-1}}{\partial A_{i,j}} &= \frac{1}{\mu} \frac{D_{v_{i,j-1}A}}{\sqrt{1 + \|D_{i,j-1}A\|_2^2 / \mu^2}}
\end{aligned}$$

and

$$\frac{\partial^2 (\varphi_\mu^{PH})_{ij}}{\partial A_{i,j}^2} = \frac{1}{\mu} \frac{2 + (D_{h_{i,j}A} - D_{v_{i,j}A})^2 / \mu^2}{(1 + \|D_{i,j}A\|_2^2 / \mu^2)^{3/2}}$$

$$\begin{aligned}
\frac{\partial^2(\varphi_\mu^{PH})_{i-1,j}}{\partial A_{i,j}^2} &= \frac{1}{\mu} \frac{1 + D_{v_{i-1,j}A}^2/\mu^2}{(1 + \|D_{i-1,jA}\|_2^2/\mu^2)^{3/2}} \\
\frac{\partial^2(\varphi_\mu^{PH})_{i,j-1}}{\partial A_{i,j}^2} &= \frac{1}{\mu} \frac{1 + D_{h_{i,j-1}A}^2/\mu^2}{(1 + \|D_{i,j-1A}\|_2^2/\mu^2)^{3/2}} \\
\frac{\partial^2(\varphi_\mu^{PH})_{ij}}{\partial A_{i+1,j} \partial A_{i,j}} &= -\frac{1}{\mu} \frac{1 + D_{v_{i,j}A}(D_{v_{i,j}A} - D_{h_{i,j}A})/\mu^2}{(1 + \|D_{i,jA}\|_2^2/\mu^2)^{3/2}} \\
\frac{\partial^2(\varphi_\mu^{PH})_{i-1,j}}{\partial A_{i-1,j} \partial A_{i,j}} &= -\frac{1}{\mu} \frac{1 + D_{v_{i-1,j}A}(D_{v_{i-1,j}A} - D_{h_{i-1,j}A})/\mu^2}{(1 + \|D_{i-1,jA}\|_2^2/\mu^2)^{3/2}} \\
\frac{\partial^2(\varphi_\mu^{PH})_{ij}}{\partial A_{i,j+1} \partial A_{i,j}} &= -\frac{1}{\mu} \frac{1 + D_{h_{i,j}A}(D_{h_{i,j}A} - D_{v_{i,j}A})/\mu^2}{(1 + \|D_{i,jA}\|_2^2/\mu^2)^{3/2}} \\
\frac{\partial^2(\varphi_\mu^{PH})_{i,j-1}}{\partial A_{i,j-1} \partial A_{i,j}} &= -\frac{1}{\mu} \frac{1 + D_{h_{i,j-1}A}(D_{h_{i,j-1}A} - D_{v_{i,j-1}A})/\mu^2}{(1 + \|D_{i,j-1A}\|_2^2/\mu^2)^{3/2}} \\
\frac{\partial^2(\varphi_\mu^{PH})_{i-1,j}}{\partial A_{i-1,j+1} \partial A_{i,j}} &= -\frac{1}{\mu} \frac{D_{h_{i-1,j}A} D_{v_{i-1,j}A}/\mu^2}{(1 + \|D_{i-1,jA}\|_2^2/\mu^2)^{3/2}} \\
\frac{\partial^2(\varphi_\mu^{PH})_{i,j-1}}{\partial A_{i+1,j-1} \partial A_{i,j}} &= -\frac{1}{\mu} \frac{D_{h_{i,j-1}A} D_{v_{i,j-1}A}/\mu^2}{(1 + \|D_{i,j-1A}\|_2^2/\mu^2)^{3/2}}
\end{aligned}$$

Then, similar arguments as in Section 2.3 can be used to obtain $\nabla Var_{PH}(\boldsymbol{\alpha})$ and $\nabla^2 Var_{PH}(\boldsymbol{\alpha})$ and further

$$\begin{aligned}
F(\boldsymbol{\alpha}) &= f(\boldsymbol{\alpha}) + \lambda Var_{PH}(\boldsymbol{\alpha}), \\
\nabla F(\boldsymbol{\alpha}) &= \nabla f(\boldsymbol{\alpha}) + \lambda \nabla Var_{PH}(\boldsymbol{\alpha}), \\
\nabla^2 F(\boldsymbol{\alpha}) &= \nabla^2 f(\boldsymbol{\alpha}) + \lambda \nabla^2 Var_{PH}(\boldsymbol{\alpha}),
\end{aligned}$$

where $f(\boldsymbol{\alpha})$, $\nabla f(\boldsymbol{\alpha})$ and $\nabla^2 f(\boldsymbol{\alpha})$ are defined in Equations (8), (18), (21), (16) and (17).

For Matlab code computing $Var_{PH}(\boldsymbol{\alpha})$, $\nabla Var_{PH}(\boldsymbol{\alpha})$ and $\nabla^2 Var_{PH}(\boldsymbol{\alpha})$, see the function *phtv* in Appendix A.

2.5 Choice of μ and λ for the total variation regularization

The parameter μ for the Huber and the pseudo Huber function was found by testing and is approximately equal to the jump in the elements of the parameter vector around the Damage 1 (see Section 3). As a rule of thumb, μ in the (pseudo) Huber controls that any variation below this value will be smoothed out and everything above μ will be possibly kept. For this reason, μ should be chosen the same for the regularized undamaged and damaged problems.

On the other hand, to find the optimal regularization parameter λ we use, when it is possible, the so-called L-curve method [23] and build a log-log-plot of the total variation norm versus the residual norm with λ as a parameter. This curve shows a trade-off between doing smoothing and data fit. In Figure 2 the L-curve is drawn for Damage 3 in Section 3 and the Huber total variation regularization with $\mu = 0.01$. In the case when only a finite number of points are known on this curve, it is popular to approximate this curve with cubic spline (red) on each line segment (blue). Then, the optimal λ corresponds to the corner of the L-curve, which is defined as the point with maximal curvature of the cubic spline approximation. It is shown that $\lambda = 0.0001$ (marked with a star) is the optimal regularization parameter. For some L-curves it was not possible to find the optimal value for λ automatically. Then the parameter λ was chosen manually around the ‘‘knee’’ of the L-curve. A couple of different values were tested for

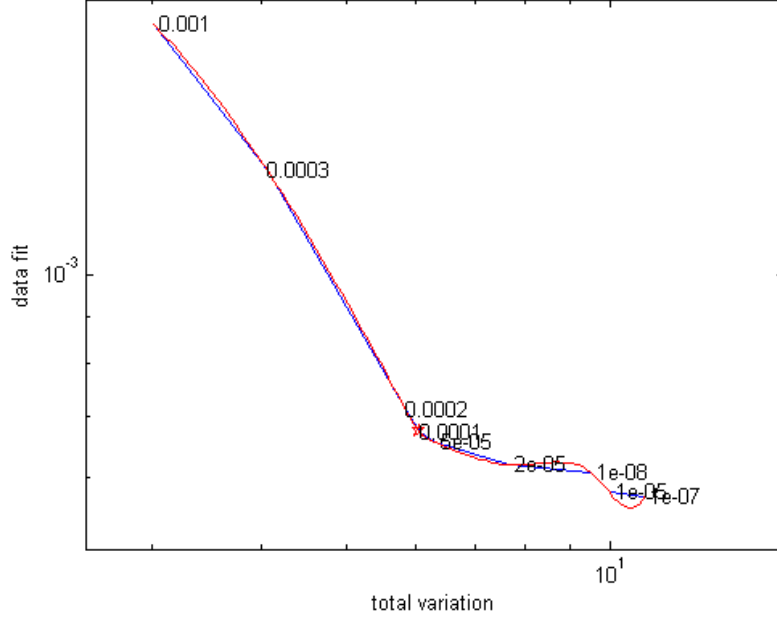


Figure 2: Log-log scale L-curve for the Huber total variation regularization problem with $\mu = 0.01$, Damage 3 in Section 3 and 65 updating parameters. The total variation corresponds to $\sum_{ij} \varphi_{\mu}^H(\|D_{ijA}\|_2)$ and data fit to $\frac{1}{2}\|\mathbf{r}(\boldsymbol{\alpha})\|_2^2$. The red line is a cubic spline approximation of each straight line segment (blue). The star corresponds to the point on the cubic spline with maximum curvature.

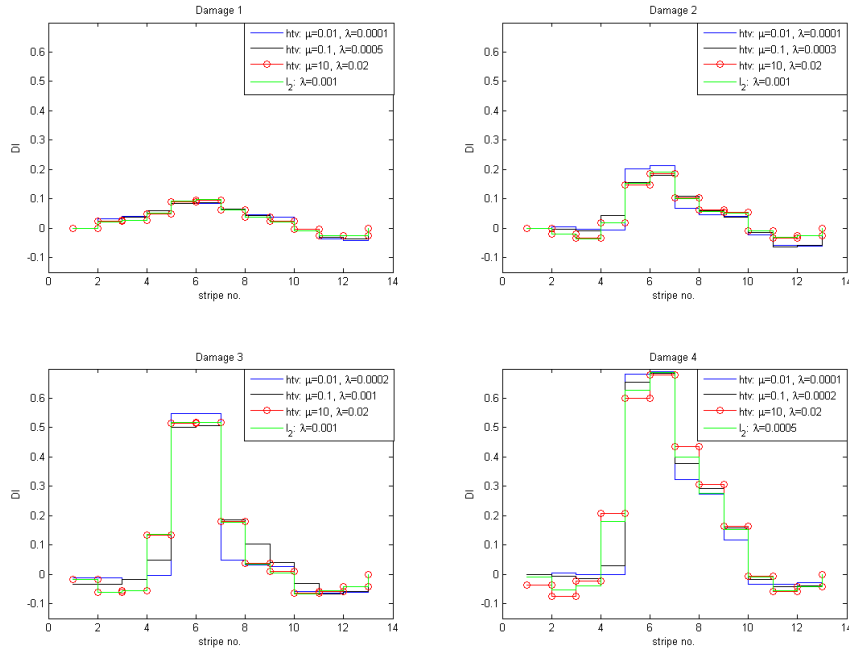


Figure 3: Comparison of the Huber total variation (htv) regularizations, 13 groups, 35.9-37.2 GPa constraints for stripe no. 1 and 13 in Figure 11 (a), 1-40 GPa constraints for stripe no. 2-12 and different values of μ .

finding one that increases the smoothing of undesired oscillations but still keeps a sharp peak that indicates a possible damage.

More robust algorithms for finding the corner of the L-curve have been developed recently (e.g. [24, 25]), but here we just use a simple solution to find an estimate of the optimal λ .

Figure 3 clearly shows that when the value of μ increases, the solution with the Huber total variation regularization becomes more similar to the solution with l_2 -norm total variation regularization as can be expected from Equation (28).

2.6 Regularization with interpolating functions

As it was mentioned before, another way to regularize the optimization problem (9) is interpolation with so-called damage functions, which was suggested and used for 1D-structures in [8, 26, 27, 28], etc. The method consists in doing the FEM updating with respect to the parameter vector α only for indices p in a subsequence $\mathcal{P} = [\mathcal{P}_1, \mathcal{P}_2, \dots, \mathcal{P}_{n_1}]$ of $[1, 2, 3, \dots, n]$ and then use interpolation for deciding the value of the remaining parameters α_p .

For example, consider a 1D-structure that is divided into 10 groups of elements with center points x_p , as illustrated in Figure 4. The blue circles indicate a coarser grid of points with indices $\mathcal{P} = [1, 4, 7, 10]$.

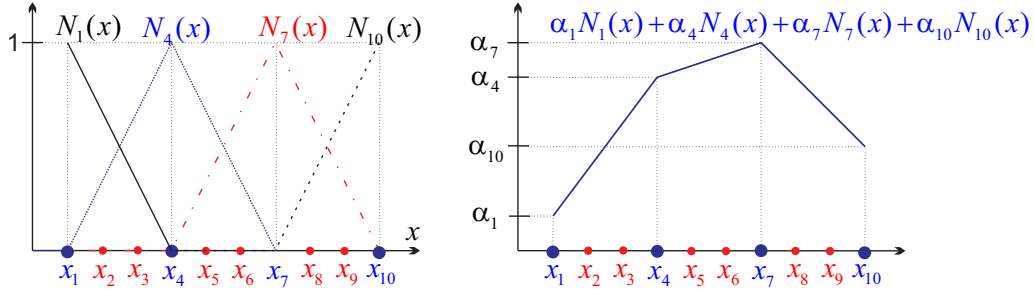


Figure 4: $N_1(x) - N_{10}(x)$ tent functions and their piecewise linear combination.

In general, let $N_{\mathcal{P}_k}(x)$ be functions with the so-called *interpolation property*

$$N_{\mathcal{P}_k}(x_{\mathcal{P}_l}) = \delta_{l,k} \stackrel{\text{def}}{=} \begin{cases} 1 & \text{if } l = k, \\ 0 & \text{if } l \neq k. \end{cases} \quad (48a)$$

Then,

$$\alpha(x) \stackrel{\text{def}}{=} \sum_{l=1}^{n_1} a_{\mathcal{P}_l} N_{\mathcal{P}_l}(x) \quad \text{and it follows that} \quad \alpha(x_{\mathcal{P}_l}) = \alpha_{\mathcal{P}_l}. \quad (48b)$$

Analogously, for a 2D-structure let $N_{\mathcal{P}_k}(x_{\mathcal{P}_l}, y_{\mathcal{P}_l})$ be functions with the interpolation property

$$N_{\mathcal{P}_k}(x_{\mathcal{P}_l}, y_{\mathcal{P}_l}) = \delta_{l,k} \quad (48c)$$

similar to (48a). Again, the optimization procedure is allowed to choose the parameters α_p freely for $p \in \mathcal{P}$. Then, all other $\alpha_p = \alpha(x_p, y_p)$ are defined as the linear interpolation by

$$\alpha(x, y) \stackrel{\text{def}}{=} \sum_{l=1}^{n_1} \alpha_{\mathcal{P}_l} N_{\mathcal{P}_l}(x, y) \quad \text{and} \quad \alpha(x_{\mathcal{P}_l}, y_{\mathcal{P}_l}) = \alpha_{\mathcal{P}_l} \text{ by (48c)}. \quad (48d)$$

The most simple choice for the 1D-case is to use piecewise linear interpolating functions $N_k(x)$ that are linear on each interval $[x_{\mathcal{P}_l}, x_{\mathcal{P}_{l+1}}]$, sometimes called *tent functions*. For instance,

see the tent functions $N_1(x) - N_{10}(x)$ and their linear combination, which indicates property (48b), plotted in Figure 4.

There are standard techniques for constructing smoother interpolating functions $N_k(x)$ with additional properties that are useful in signal processing [29, Section 3.1]. This would however not make any practical difference for the relatively small number of groups of elements used for the the concrete plate in Section 3.

For a 2D-structure we have tried two simple solutions. Firstly, we have generalized the interpolating functions to a 2D-grid similar to the suggestions in [30]. This generalization works for structures with group center points arranged in a rectangular grid. For other geometries further generalizations of this solution are needed. Secondly, we take the interpolating functions equal to *triangular element shape functions* as they are defined in the FEM literature [31]. These functions show superiority over the rectangular element interpolating functions due to much less restrictions on the points in the 2D grid on which they are defined. For our test case in Section 3 the results of these two solutions were pretty similar and only a bit better smoothing was achieved for the rectangular element interpolating functions used in our plots.

Consider the case with the triangular element shape functions. Suppose that we have $P = 25$ updating parameters a_p in points (x_p, y_p) , ordered in a grid

$$\begin{array}{ccccc}
 a_1 & a_6 & a_{11} & a_{16} & a_{21} \\
 a_2 & a_7 & a_{12} & a_{17} & a_{22} \\
 a_3 & a_8 & a_{13} & a_{18} & a_{23} \\
 a_4 & a_9 & a_{14} & a_{19} & a_{24} \\
 a_5 & a_{10} & a_{15} & a_{20} & a_{25}
 \end{array} \tag{49}$$

with blue color for the parameters of the coarse grid. Now the coarse grid indices are

$$\mathcal{P} = [1, 3, 5, 11, 13, 15, 21, 23, 25] \stackrel{\text{def}}{=} [\mathcal{P}_1, \mathcal{P}_2, \dots, \mathcal{P}_9].$$

We use the Delaunay triangulation [32] of the set of points $x_{\mathcal{P}_i}$ organized in an almost regular 2D grid similar to the one in (49). Then, for each point (x, y) in the triangle Δ with vertices at points (x_i, y_i) , (x_j, y_j) and (x_k, y_k) with area

$$S(\Delta) = \frac{1}{2} \det \begin{vmatrix} 1 & x_i & y_i \\ 1 & x_j & y_j \\ 1 & x_k & y_k \end{vmatrix}.$$

we define three triangular element shape functions (see Figure 5) as follows

$$\begin{aligned}
 N_i^\Delta(x, y) &= \frac{1}{2S(\Delta)} (a_i + b_i x + c_i y) \\
 N_j^\Delta(x, y) &= \frac{1}{2S(\Delta)} (a_j + b_j x + c_j y) \\
 N_k^\Delta(x, y) &= \frac{1}{2S(\Delta)} (a_k + b_k x + c_k y),
 \end{aligned}$$

where

$$a_i = x_j y_k - x_k y_j \quad b_i = y_j - y_k \quad c_i = x_k - x_j$$

and so on, with a cyclic permutation of subscripts in the order i, j and k .

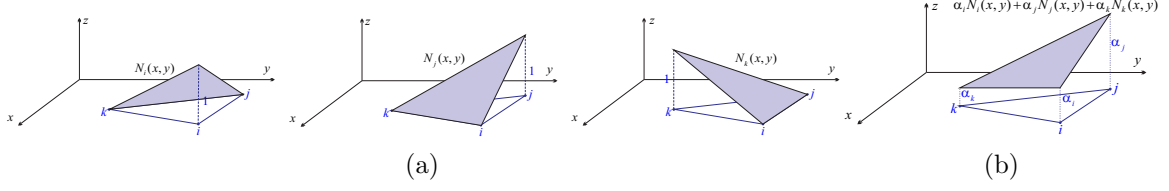


Figure 5: (a) Triangular element shape functions $N_i(x, y)$, $N_j(x, y)$ and $N_k(x, y)$ for triangle ijk . (b) Their linear combination over triangle ijk .

Let L be the $n \times n_1$ -matrix

$$L \stackrel{\text{def}}{=} (\mathbf{N}_{\mathcal{P}_1} \quad \mathbf{N}_{\mathcal{P}_2} \quad \cdots \quad \mathbf{N}_{\mathcal{P}_{n_1}}) \quad \text{with} \quad \mathbf{N}_l \stackrel{\text{def}}{=} \begin{pmatrix} \tilde{N}_l(x_1, y_1) \\ \tilde{N}_l(x_2, y_2) \\ \vdots \\ \tilde{N}_l(x_n, y_n) \end{pmatrix} \quad \text{and} \quad \tilde{N}_l = \bigcup_{\Delta_k: l \text{ vertex of } \Delta_k} N_l^{\Delta_k}. \quad (50)$$

If $\boldsymbol{\alpha}^{\mathcal{P}}$ is the vector of the updating parameters in the coarse grid, then (48d) and (50) give that

$$\boldsymbol{\alpha} = L\boldsymbol{\alpha}^{\mathcal{P}}. \quad (51)$$

Moreover, the updated $m \times n_1$ Jacobian, which now can be used in Equations (16) and (17) is

$$\mathbf{J}_r(\boldsymbol{\alpha}^{\mathcal{P}}) = \mathbf{J}_r(\boldsymbol{\alpha})L, \quad (52)$$

since by (51)

$$(\mathbf{J}_r(\boldsymbol{\alpha}^{\mathcal{P}}))_{d,l} \stackrel{\text{def}}{=} \frac{\partial r_d}{\partial \alpha_{\mathcal{P}_l}} = \sum_{p=1}^n \frac{\partial r_d}{\partial \alpha_p} \frac{\partial \alpha_p}{\partial \alpha_{\mathcal{P}_l}} = \sum_{p=1}^n (\mathbf{J}_r(\boldsymbol{\alpha}))_{d,p} \frac{\partial (L\boldsymbol{\alpha}^{\mathcal{P}})_p}{\partial \alpha_{\mathcal{P}_l}} = \sum_{p=1}^n (\mathbf{J}_r(\boldsymbol{\alpha}))_{d,p} L_{p,l}.$$

3 Test case

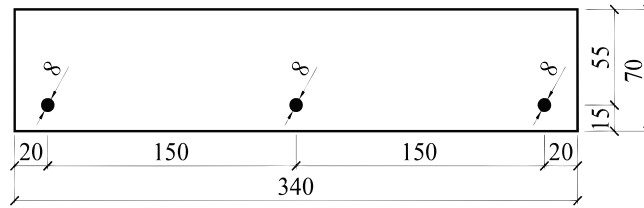


Figure 6: Cross-section of the test plate (unit: mm).

Measurements of forced vibrations were performed on a $1050 \times 340 \times 70$ mm concrete plate, reinforced by three steel rebars of 8 mm diameter, positioned as in Figure 6. The plate was excited by a swept sine force signal using an electromagnetic shaker of type LDS V406 combined with an amplifier LDS PA100E. Ideally, either the plate or the shaker should be freely supported (or grounded) [33, Section 3.3]. The plate was therefore hanging in bungee cords as shown in Figure 7. The input force and the corresponding driving point acceleration were measured by an impedance head, Brüel & Kjær 8001, each signal connected through a charge amplifier B&K 2635. The remaining response points were measured using accelerometers of type B&K 4508



Figure 7: The measurement setup.

B002, which were attached to the structure by using mounting plastic clips B&K UA-1407 together with a thin layer of beeswax applied inside the clips for a more firm connection. The accelerometers/clips were glued to the plate at $5 \times 13 = 65$ measurement points. A B&K 3560-C served as the data acquisition unit. It was controlled by a portable PC by using the software B&K Pulse Labshop. These measurements were done for the following five cases

Damage 0 Undamaged plate.

Damage 1 A 7 mm deep notch cut with an angle grinder.

Damage 2 A 13.5 mm deep notch cut with an angle grinder.

Damage 3 Deeper real cracks, produced by applying a 6,6 kN linear load, as shown in Figure 8 (a).

Damage 4 Even deeper cracks (Figure 9), produced by using C-clamps to apply larger linear loads.

By using FRF analysis, totally 12 mode shapes were identified from the measurement data, but only the first three bending mode shapes (see Figure 10 and Table 1) were used in the damage identification. The 30 first modes were used in the finite element analysis in order to produce

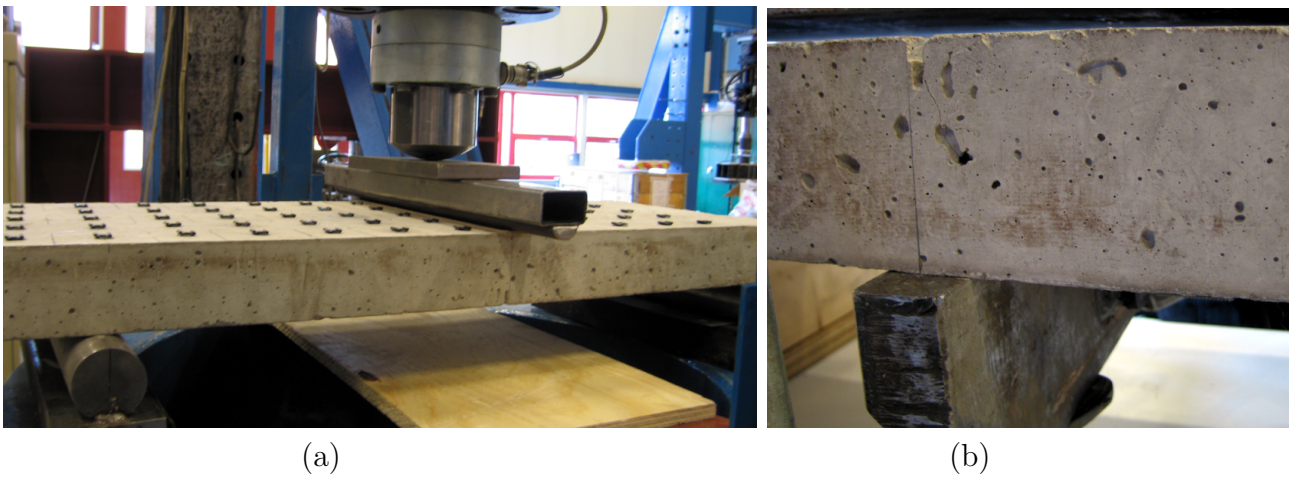


Figure 8: (a) Linear 6.6 kN load for producing deeper cracks located at the notch. (b) Visible deeper crack after the largest applied linear load (Damage 4).

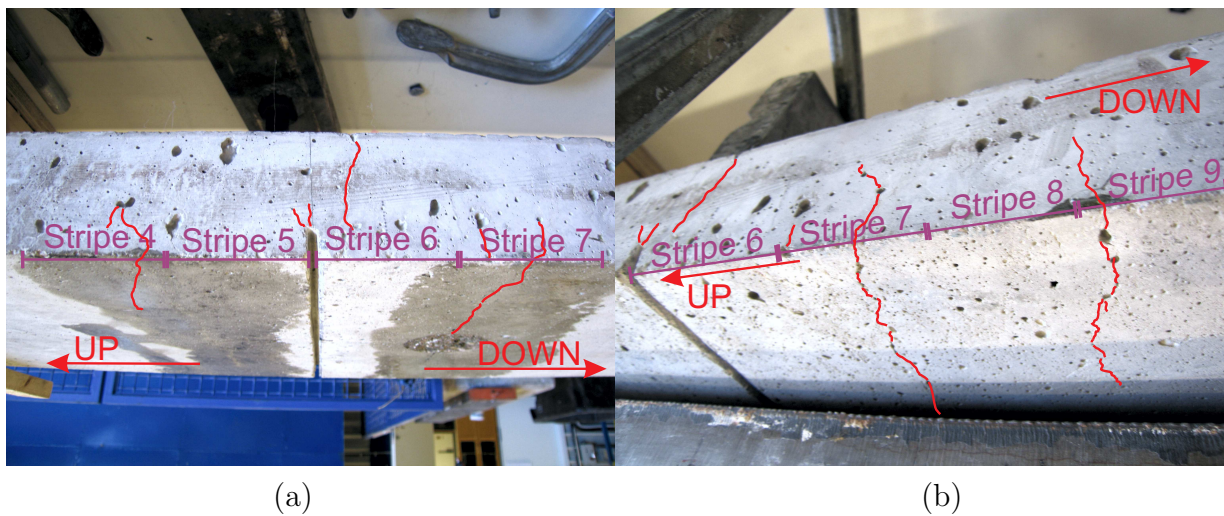


Figure 9: Visible cracks on the plate after applying larger linear loads with C-clamps. The left-most crack in (a) and the right-most crack in (b) seemed to be less deep.

system matrices and compute modal data derivatives with respect to the updating parameters in (23b).

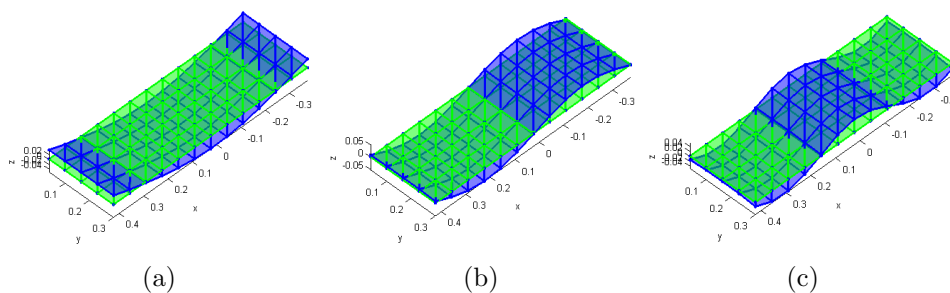


Figure 10: The first three measured bending mode shapes. Green color corresponds to the undeformed plate. (a) Mode shape no. 1: eigenfrequency $f = 249.03 \pm 0.11$ Hz. (b) Mode shape no. 3: $f = 668.40 \pm 0.52$ Hz. (c) Mode shape no. 5: $f = 1269.88 \pm 0.38$ Hz.

Mode	Undamaged plate	Damage 1	Damage 2	Damage 3	Damage 4
Mode 1	249.03 ± 0.11	243.00 ± 0.11	239 ± 0.10	217.13 ± 0.60	192.60 ± 0.54
Mode 3	668.40 ± 0.52	660.99 ± 0.92	661.48 ± 0.22	638.24 ± 0.57	604.20 ± 0.28
Mode 5	1269.88 ± 0.38	1256.97 ± 0.80	1257.13 ± 0.94	1221.70 ± 0.58	1159.06 ± 0.53

Table 1: Eigenfrequencies (in Hertz with standard deviation) for the first 3 bending mode shapes for both undamaged and damaged cases.

3.1 Summary of results

We have compared the results of FEMU for an 1D (wide beam) and 2D plate models and different regularization techniques. The 1D and 2D plate models were divided into 13 and 65 groups, respectively, as shown on Figure 11.

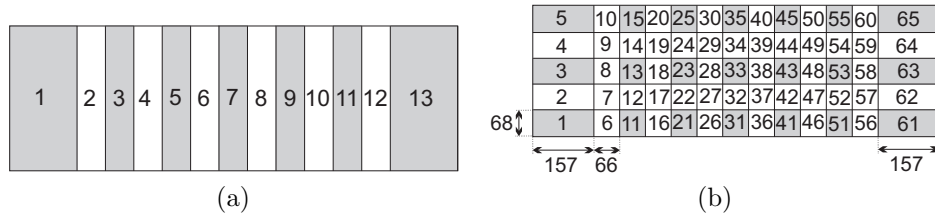


Figure 11: Plate division into groups. Grey color corresponds to the coarse mesh grid used for regularization by interpolation. (a) 13 groups. (b) 65 groups (unit: mm).

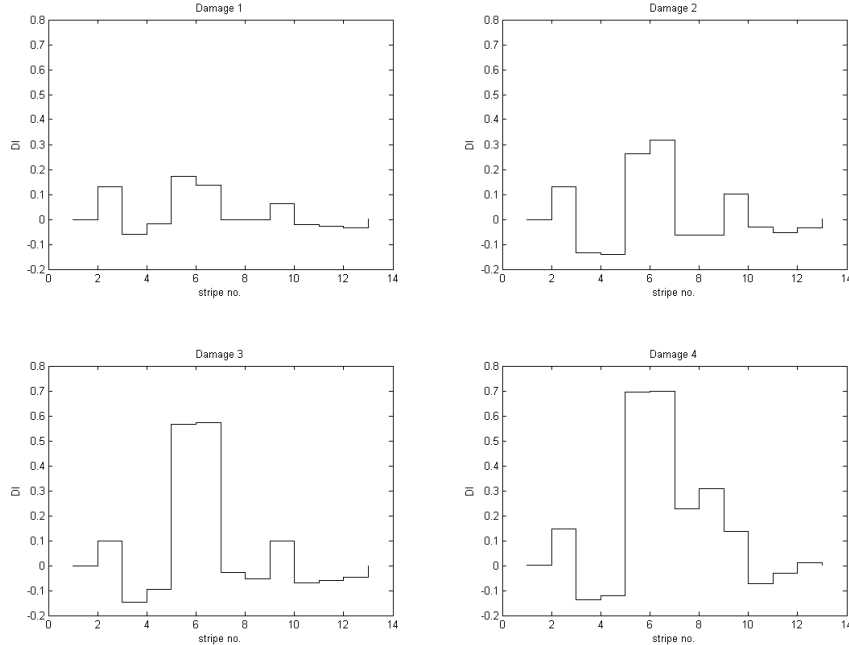


Figure 12: No regularization, 13 groups, 35.9–37.2 GPa constraints for the stripes no. 1 and 13, 1–40 GPa constraints for stripes no. 2–12.

The plotted parameter is the damage index, that is, $\alpha_i = DI_i = \frac{E_i^0 - E_i}{E_i^0}$, where E_i is the updated elasticity modulus and E_i^0 its initial value for the i^{th} group. Thus, the damages are

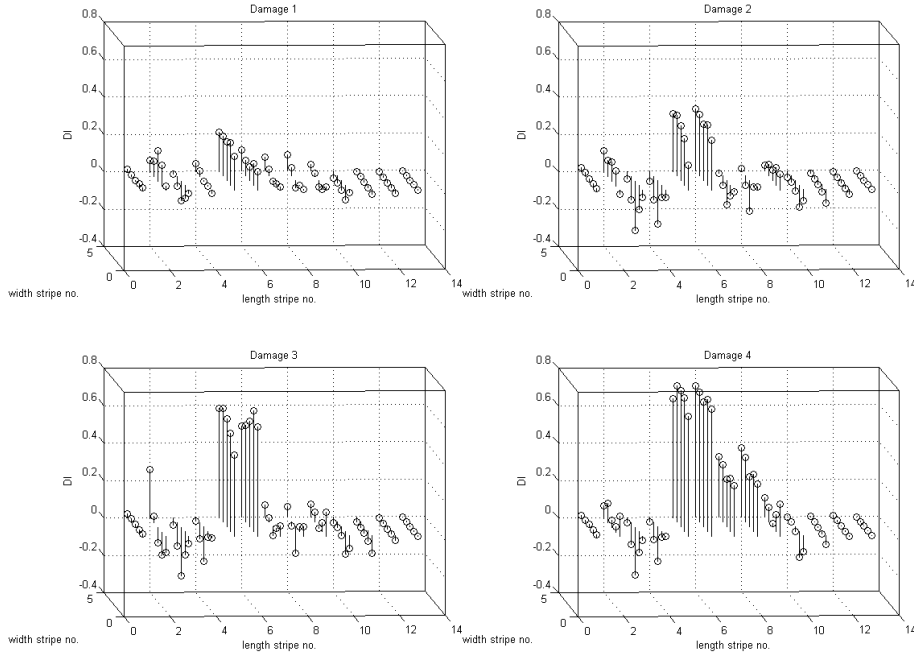


Figure 13: No regularization, 65 groups, 35.9–37.2 GPa constraints for short edges, 1–40 GPa constraints for the remaining groups.

indicated by high DI_i values.

For all presented results, the elasticity modulus in the groups containing the two shorter edges are constrained to the range 35.9–37.2 GPa, which corresponds to maximal damage index $DI_i \approx 0.02$. This was suggested in [8] for avoiding unrealistic high parameter values at edges, due to lower sensitivity of modal data to changes in elasticity modulus there.

Damages 1 and 2 (the notches) are located exactly between stripes number 5 and 6 in Figure 11. For Damage 4, additional cracks were visible closer to and along the center line in stripe number 7, see Figure 9. Thus the known damages are in the interval 5–8 and some smaller cracks in stripe 4 and 9.

The results obtained without regularization (see Figures 12 and 13) show clearly an oscillating pattern for the damage indices, from which is it quite difficult to correctly identify both the location and severity of the damage. The damage index peaks around the real damages, but there are also additional oscillations and peaks at stripes 2 and 9.

From Figure 14, we see that for the small damage, i.e. Damage 1 in our case, different regularization techniques result in almost the same damage pattern, which can be described as a bell shaped parameter distribution around the damage location at position between stripes 5 and 6. On the other hand, when the damage becomes to be more pronounced, the optimization with the Huber total variation regularization results in a more localized damage pattern compared with the results based on either the damage functions or l_2 -norm total variation techniques. The fact that the test cases started with a well-localized notch (cut) damage supports this type of damage pattern compared with more smeared bell shaped pattern.

Figure 15 shows almost the same comparison of methods as in Figure 14 but for the 2D plate model and 65 groups. Here there is a bigger difference between the results for the interpolation with the damage functions suggested in [30] and those for the Huber total variation. Huber total variation gives a sharp damage indication in stripes 5–6 for Damage 2–3, corresponding

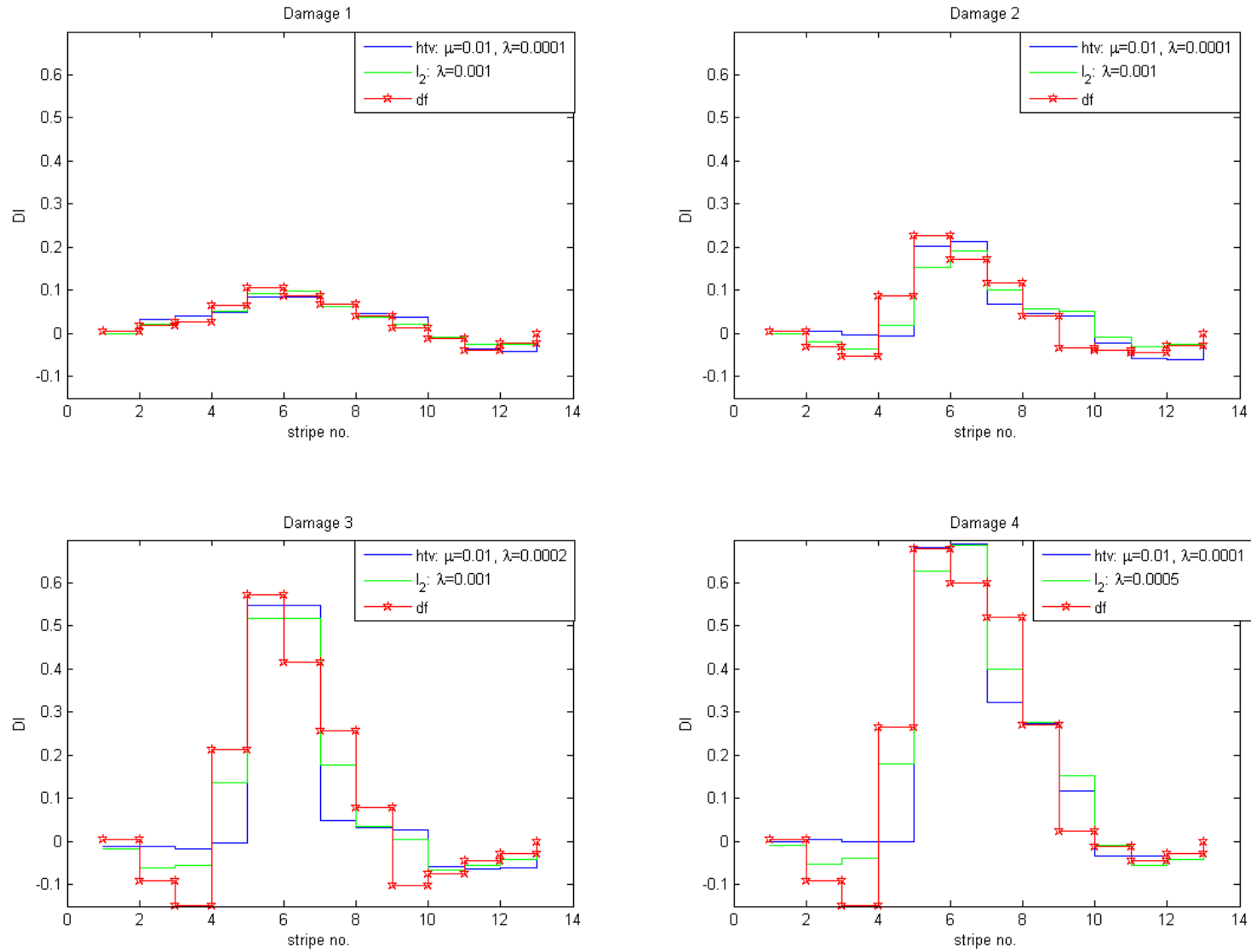


Figure 14: Comparison of damage functions (df), l_2 -norm and Huber total variation (htv) regularizations, 13 groups, 35.9-37.2 GPa constraints for stripe no. 1 and 13, 1-40 GPa constraints for stripe no. 2-12.

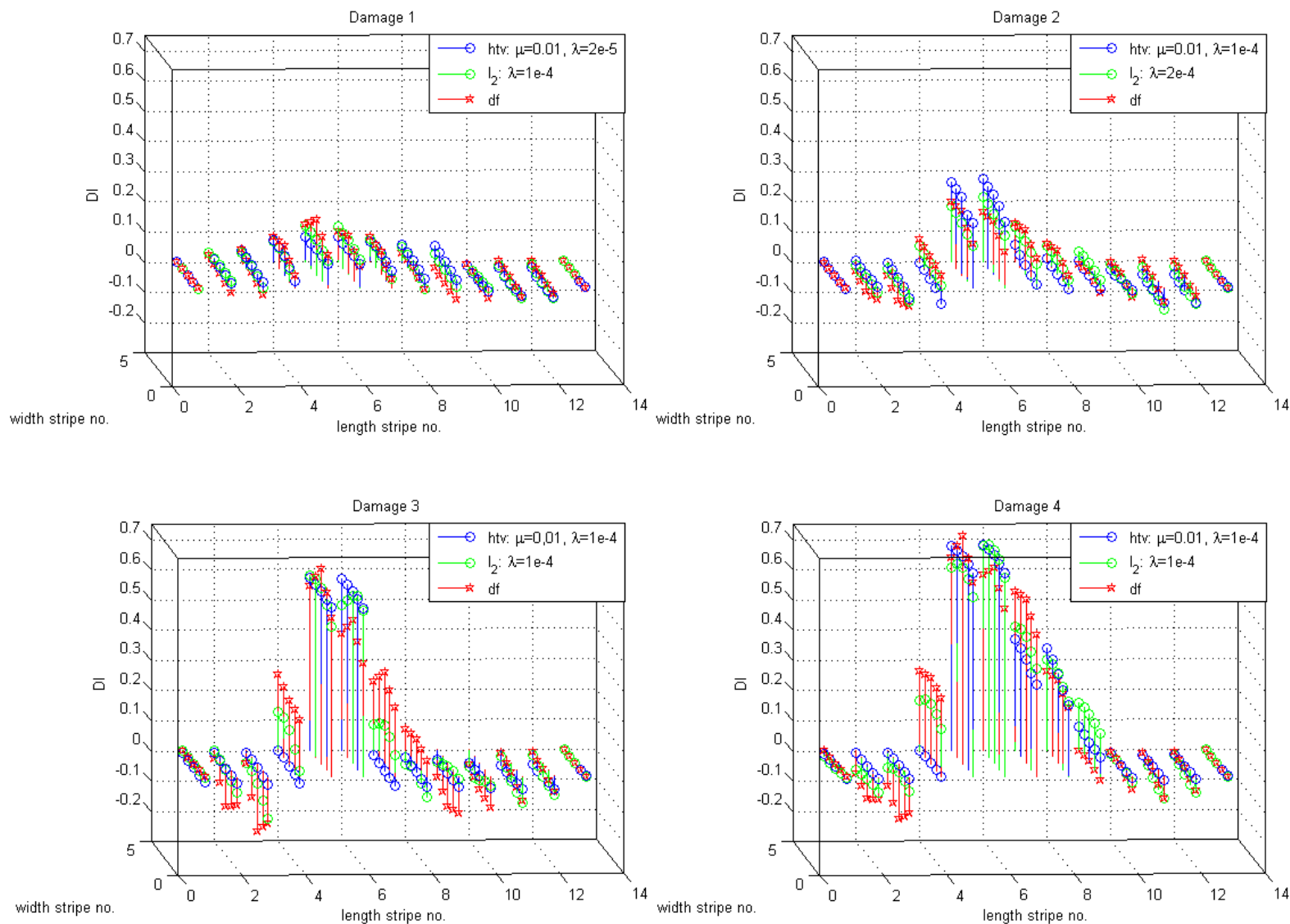


Figure 15: Comparison of damage functions (df), l_2 -norm and Huber total variation (htv) regularizations, 65 groups, 35.9-37.2 GPa constraints on short edges, 1-40 GPa constraints for the remaining groups. For the damage functions the coarse mesh grid is [1 3 5 11 13 15 21 23 25 31 33 35 41 43 45 51 53 55 61 63 65].

to the notch and cracks located between these stripes, whereas for Damage 4, it also gives some indication in stripes 7–9, corresponding to the additional cracks in Figure 9 (b). It gives no indication of the small cracks in Stripe 4 in Figure 9 (b), however, which could mean that those cracks are less deep than the others. The Huber penalty term also reduces small amplitude oscillations in the updating parameters. See the differences between the methods at stripes 2–4, 5–6 and 7–12 for Damage 2–4 in Figure 15.

The l_2 -norm total variation and the damage function regularization, on the other hand, both have the damage identification spread out over stripes 4–9 for all four damages. It is then more difficult to judge whether this indicates a spread out damage or whether it is the smoothing inherent in these methods. For a less well-localized damage, like Damage 4, all of the above methods give more similar results.

We have also compared Huber and pseudo Huber total variation regularization. The results of these two methods are quite similar for 65 groups and therefore are not presented here. These computations are performed in order to justify the results obtained with the Huber total variation regularization, for which it is more easy to motivate the choice of the threshold parameter μ but which fails to have the continuous second-order derivative required in computations.

4 Conclusions

We have compared two different approaches for the regularization in FEMU. Interpolation based regularization, on the one hand, gives an automatic smoothing of the computed updating parameters at the cost of less precise localization of the damage. Regularization with (pseudo) Huber total variation penalty term, on the other hand, depends on a not fully automatic choice of parameters μ and λ , but results in a more precise localization and identified severity of a well-localized damage. An inherent advantage of the (pseudo) Huber penalty term is that it also reduces small amplitude oscillations in the updating parameters. All investigated methods give more similar results for a less well-localized damage.

5 Further work

Regularization with penalty term depends on choosing the regularization parameter λ . The L-curve and its approximation with the cubic spline does not always give an automatic choice of the optimal λ , so a better method for finding the optimal λ would be desired. It would also be necessary to understand better the impact of noise on the total variation regularization methods for which a numerical finite element model could make a contribution. It could also be interesting to apply this method to a real structure, e.g. a bridge.

Acknowledgements

We gratefully acknowledge our colleges at LTU: Inge Söderkvist for a number of valuable discussions around the regularization techniques, Fredrik Ljungren for the help with vibration tests, Lennart Elfgrén, Ulf Ohlsson and Zheng Huang for the discussion about the effects of damage on the structures.

A Matlab code

```
function [res,J] = l2tv(a,r,c)
% Builds a rectangular (r x c) grid A for the parameter vector a and
```



```

% then transforms it into the residual vector and the Jacobian of the
% residual at A for further use in the least squares estimation.
% This works both for 1D (r==1 or c==1) and 2D cases (r>1 and c>1).
%
% INPUT:
% a - column vector of the parameters
% r - number of rows in the 2D grid
% c - number of columns in the 2D grid
%
% OUTPUT:
% res - residual vector corresponding to A
% J - Jacobian of the residual vector at A

n = length(a);
if n~=r*c
    error('Error in grid dimension!')
end
A = reshape(a,r,c);

Dh = diff(A,[],1);
Dv = diff(A,[],2);
DDh = [];
DDv = [];

if r>1
    Dr = toeplitz([-1,zeros(1,r-2)],[-1,1,zeros(1,r-2)]);
    DDh = kron(eye(c),Dr);
end
if c>1
    DDv = toeplitz([-1,zeros(1,n-r-1)],[-1,zeros(1,r-1),1,zeros(1,n-r-1)]);
end
res = [Dv(:); Dh(:)];
J = [DDv; DDh];

function [f,grad,hess] = htv(a,r,c,mu)
% Computes the value, gradient and Hessian of
% the Huber total variation at A=reshape(a,r,c).
% Huber total variation is defined as follows
%  $\text{Var\_phi}(A) = \sum_{ij} \text{phi}(\sqrt{(A_{i+1,j}-A_{i,j})^2 + (A(i,j+1)-A_{i,j})^2})$ ),
% where phi is the Huber function given by
%  $\text{phi}(x)=x^2/(2\mu)$  for  $|x|\leq\mu$  and  $\text{phi}(x)=|x|-\mu/2$  for  $|x|>\mu$ 
% and mu is a predefined threshold parameter.
%
% INPUT
% a - column vector of the parameters
% r - number of rows in the 2D grid
% c - number of columns in the 2D grid, c>1
% mu - threshold parameter for the Huber function
%

```

```

% OUTPUT:
% f - value of the Huber total variation at vector a
%     organized into rectangular (r x c) grid A
% grad - gradient of Huber total variation at A
% hess - Hessian of Huber total variation at A

if c==1
    % Transpose to row vector:
    c=r; r=1;
end

A = reshape(a,r,c);

Dh = diff(A,[],1);
Dh = [Dh;zeros(1,c)];
Dv = diff(A,[],2);
Dv = [Dv zeros(r,1)];

X = sqrt(Dh.^2+Dv.^2);
F = (X<=mu).*(X.^2/(2*mu))+(X>mu).*(X-mu/2);
f = sum(sum(F));

H= (X<=mu).*Dh/mu;
V = (X<=mu).*Dv/mu;
Hs = zeros(size(H));
Vs = zeros(size(H));
Hs(X>mu) = Dh(X>mu)./X(X>mu);
Vs(X>mu) = Dv(X>mu)./X(X>mu);

Y = X.^3;
H2 = zeros(size(H));
V2 = zeros(size(H));
HV = zeros(size(H));
C = (X<=mu).*1/mu;
H2(X>mu) = Dh(X>mu).^2./Y(X>mu);
V2(X>mu) = Dv(X>mu).^2./Y(X>mu);
HV(X>mu) = Dh(X>mu).*Dv(X>mu)./Y(X>mu);

if r>1
    H0r(2:r,1:c) = H(1:r-1,1:c);
    Hs0r(2:r,1:c) = Hs(1:r-1,1:c);
    C0r(2:r,1:c) = C(1:r-1,1:c);
    V20r(2:r,1:c) = V2(1:r-1,1:c);
    HV0r(2:r,1:c) = HV(1:r-1,1:c);
else
    H0r=0;Hs0r=0;C0r=0;V20r=0;HV0r=0;
end

```

```

if c>1
    V0c(1:r,2:c) = V(1:r,1:c-1);
    Vsq0c(1:r,2:c) = Vs(1:r,1:c-1);
    C0c(1:r,2:c) = C(1:r,1:c-1);
    H20c(1:r,2:c) = H2(1:r,1:c-1);
else
    V0c=0;Vsq0c=0;C0c=0;H20c=0;
end

grad = -H-V-Hs-Vs+H0r+Hs0r+V0c+Vsq0c;
grad = grad(:);

% (k,k) main diagonal of the Hessian
tmp = 2*C+H2-2*HV+V2+C0r+V20r+C0c+H20c;
hess = diag(tmp(:));

% (k,k+1) diagonal of the Hessian
tmp2 = -C+HV-V2;
tmp2(r,:) = zeros(1,c);
hess(r*c+1:r*c+1:end) = hess(r*c+1:r*c+1:end)+tmp2(1:r*c-1);

% (k,k+r) diagonal of the Hessian
tmp3 = -C+HV-H2;
tmp3(:,c) = []; % size(tmp3) = (r,c-1)
hess(r*c*r+1:r*c+1:end) = hess(r*c*r+1:r*c+1:end)+tmp3(1:end);

% (k,k+r-1) diagonal of the Hessian
tmp4 = -HV0r;
tmp4(:,c) = zeros(r,1);
hess(r*c*(r-1)+1:r*c+1:end) = hess(r*c*(r-1)+1:r*c+1:end)+tmp4(1:r*c-(r-1));
hess = hess + triu(hess,1)';

function [f,grad,hess] = phtv(a,r,c,mu)
% Computes the value, gradient and Hessian of
% the pseudo Huber total variation at A=reshape(a,r,c).
% Pseudo Huber total variation is defined as follows
%  $\text{Var\_phi}(A) = \sum_{ij} \text{phi}(\sqrt{(A_{i+1,j}-A_{i,j})^2 + (A_{i,j+1}-A_{i,j})^2})$ ),
% where phi is the pseudo Huber function given by
%  $\text{phi}(x)=\mu(\sqrt{1+(x/\mu)^2}-1)$  and mu is a predefined threshold parameter.
%
% INPUT
% a - column vector of the parameters
% r - number of rows in the 2D grid
% c - number of columns in the 2D grid, c>1
% mu - threshold parameter for the pseudo Huber function
%
% OUTPUT:
% f - value of the pseudo Huber total variation at vector a
%     organized into rectangular (r x c) grid A

```

```

% grad - gradient of pseudo Huber total variation at A
% hess - Hessian of pseudo Huber total variation at A

if c==1
    % Transpose to row vector:
    c=r; r=1;
end
A = reshape(a,r,c);

Dh = diff(A, [],1);
Dh = [Dh;zeros(1,c)];
Dv = diff(A, [],2);
Dv = [Dv zeros(r,1)];

f = sum(sum(mu*(sqrt(1+(Dh.^2+Dv.^2)/mu^2)-1)));

X = sqrt(1+(Dh.^2+Dv.^2)/mu^2);
H = 1/mu*Dh./X;
V = 1/mu*Dv./X;
Y = mu*X.^3;
H2 = 1/mu^2*Dh.^2./Y;
V2 = 1/mu^2*Dv.^2./Y;
HV = 1/mu^2*Dh.*Dv./Y;
C = 1./Y;

if r>1
    H0r(2:r,1:c) = H(1:r-1,1:c);
    C0r(2:r,1:c) = C(1:r-1,1:c);
    V20r(2:r,1:c) = V2(1:r-1,1:c);
    D(2:r,1:c) = -HV(1:r-1,1:c);
else
    H0r=0;C0r=0;V20r=0;D=zeros(r,c);
end
if c>1
    V0c(1:r,2:c) = V(1:r,1:c-1);
    C0c(1:r,2:c) = C(1:r,1:c-1);
    H20c(1:r,2:c) = H2(1:r,1:c-1);
else
    V0c=0;C0c=0;H20c=0;
end

grad = -H-V+H0r+V0c;
grad = grad(:);

% (k,k) diagonal of the Hessian
diag1 = 2*C+H2-2*HV+V2+C0r+V20r+C0c+H20c;
hess = diag(diag1(:));

```

```

% (k,k+1) diagonal of the Hessian
diag2 = -C-V2+HV;
diag2(r,:) = zeros(1,c);
hess(r*c+1:r*c+1:end) = hess(r*c+1:r*c+1:end)+diag2(1:r*c-1);

% (k,k+r) diagonal of the Hessian
diag3 = -C-H2+HV;
diag3(:,c) = []; % size(diag3) = (r,c-1)
%diag3 = diag3'; diag3 = diag3(:);
hess(r*c*r+1:r*c+1:end) = hess(r*c*r+1:r*c+1:end)+diag3(1:r*(c-1));

% (k,k+r-1) diagonal of the Hessian
diag4 = D;
hess(r*c*(r-1)+1:r*c+1:end) = hess(r*c*(r-1)+1:r*c+1:end)+diag4(1:r*c-(r-1));

hess = hess + triu(hess,1)';

```

References

- [1] S. W. Doebling, C. R. Farrar, and M. B. Prime. A summary review of vibration-based damage identification methods. *Shock Vib*, 30(2):91–105, March 1998. WWW: http://http://public.lanl.gov/prime/doebling_svd.pdf.
- [2] John E. Mottershead, Michael Link, and Michael I. Friswell. The sensitivity method in finite element model updating: A tutorial. *Mech. Sys. Sig. Proc.*, 25(7):2275–2296, October 2011. DOI: 10.1016/j.ymsp.2010.10.012.
- [3] Tshilidzi Marwala. *Finite Element Model Updating Using Computational Intelligence Techniques: Applications to Structural Dynamics*. Kluwer Academic, 2010.
- [4] H. G. Natke. Updating computation models in the frequency domain based on measured data: survey. *Probabilist. Eng. Mech.*, 3(1):28–35, 1988.
- [5] M.I. Friswell and J.E. Mottershead. *Finite Element Model Updating in Structural Dynamics*. Kluwer Academic, Dordrecht, 1995.
- [6] M. Link. Updating of analytical models - review of numerical procedures and application aspects. *In book Structural Dynamics 2000: current status and future directions*, pages 193–223, 2001.
- [7] M.I. Friswell, J. E. Mottershead, and H. Ahmadian. Finite-element model updating using experimental test data: parametrization and regularization. *Phil. Trans. R. Soc. Lond. A*, 359:169–186, 2001. DOI: 10.1098/rsta.2000.0719.
- [8] Anne Teughels, Johan Maeck, and Guido De Roeck. Damage assessment by FE model updating using damage functions. *Comput Struct*, 80(25):1869–1879, September 2002. DOI: 10.1016/S0045-7949(02)00217-1.
- [9] B. Weber, P. Paultre, and J. Proulx. Consistent regularization of nonlinear model updating for damage identification. *Mech. Sys. Sig. Proc.*, 23:1965–1985, 2009.

- [10] J. Lemaitre and R. Desmorat. *Engineering Damage Mechanics. Ductile, Creep, Fatigue and Brittle Failures*. Springer, Berlin, 2005.
- [11] J. Dattorro. *Convex optimization & Euclidean distance geometry*. Meboo Publishing USA, 2005.
- [12] Rune Brincker and Carlos Ventura. *Introduction to Operational Modal Analysis*. Wiley, August 2015. WWW: <http://eu.wiley.com/WileyCDA/WileyTitle/productCd-111996315X.html>.
- [13] R. J. Allemang and D. L. Brown. A correlation coefficient for modal vector analysis. In *Proceedings of the First International Modal Analysis Conference*, pages 110–116, Orlando, FL, 1982. Union College, Schenectady, NY.
- [14] R. J. Allemang. The modal assurance criterion (MAC): twenty years of use and abuse. *J. Sound Vib.*, 37(8):14–23, 2003.
- [15] R. L. Fox and R. M. Kapoor. Rate of change of eigenvalues and eigenvectors. *AIAA J.*, 6(12):2426–2429, December 1968.
- [16] MATLAB. MATLAB optimization toolbox user’s guide. version 7.2 (R2015a). Technical report, The Mathworks, 2015. WWW: http://www.mathworks.com/help/pdf_doc/optim/optim_tb.pdf.
- [17] L. I. Rudin, S. Osher, and Fatemi E. Nonlinear total variation based noise removal algorithms. *Physica D*, 60(1-4):259–268, 1992. DOI: 10.1016/0167-2789(92)90242-F.
- [18] S. Boyd and L. Vandenberghe. *Convex Optimization*. Cambridge University Press New York, Boston ; Basel, 2004.
- [19] I. Loris and C. Verhoeven. Iterative algorithms for total variation-like reconstructions in seismic tomography. *GEM*, 3(2):179–208, 2012. DOI: 10.1007/s13137-012-0036-3.
- [20] G. Chavent and K. Kunisch. Regularization of linear least squares problems by total bounded variation. *ESAIM Control Optim. Calc. Var.*, 2:359–376, 1997. DOI: 10.1006/gmip.1995.1043.
- [21] P. J. Huber. Robust estimation of a location parameter. *Ann. Statist.*, 35(1):73–101, 1964. DOI: 10.1214/aoms/1177703732.
- [22] Richard Hartley and Andrew Zisserman. *Multiple View Geometry in Computer Vision*. Cambridge University Press, second edition, 2003.
- [23] P. C. Hansen and D. P. O’Leary. The use of the L-curve in the regularization of discrete ill-posed problems. *SIAM J. Sci. Comput.*, 14(6):1487–1503, August 1993. DOI: 10.1137/0914086.
- [24] J. L. Castellanos and V. G. Gómez. The triangle method for finding the corner of the L-curve. *Appl. Numer. Math.*, 43(4):359 – 373, 2002. DOI: 10.1016/S0168-9274(01)00179-9.
- [25] P. C. Hansen, Jensen T. K., and Rodriguez G. An adaptive pruning algorithm for the discrete L-curve criterion. *J. Comput. Appl. Math.*, 198(2):483 – 492, 2007. DOI: 10.1016/j.cam.2005.09.026.

- [26] Anne Teughels and Guido De Roeck. Damage assessment of the Z24 bridge by FE model updating. *Key Eng. Mat.*, 245–246:19–26, July 2003. DOI: 10.4028/www.scientific.net/KEM.245-246.19.
- [27] Anne Teughels and Guido De Roeck. Damage detection and parameter identification by finite element model updating. *Arch. Comput. Meth. Engng.*, 12(2):123–164, June 2005. DOI: 10.1007/BF03044517.
- [28] Edwin Reynders, Anne Teughels, and Guido De Roeck. Finite element model updating and structural damage identification using OMAX data. *Mech. Sys. Sig. Proc.*, 24(5):1306–1323, July 2010. DOI: 10.1016/j.ymsp.2010.03.014.
- [29] Stefan Ericsson and Niklas Grip. Using a natural deconvolution for analysis of perturbed integer sampling in shift-invariant spaces. *J. Math. Anal. Appl.*, 373(1):271–286, January 2011. DOI: 10.1016/j.jmaa.2010.07.021, WWW: http://pure.ltu.se/portal/files/4961764/ErGr11a_preprint.pdf.
- [30] Wei Song, Shirley Dyke, GunJin Yun, and Thomas Harmon. Improved damage localization and quantification using subset selection. *J Eng Mech-ASCE*, 135(6):548–560, June 2009. DOI: 10.1061/(ASCE)EM.1943-7889.0000005.
- [31] O. C. Zienkiewicz and R. L. Taylor. *The Finite Element Method. Volume 1: The Basis*, volume 1. McGraw-Hill, 5 edition, 2005.
- [32] MATLAB (R2015b), 2015. WWW: <http://se.mathworks.com/help/matlab/ref/delaunay.html>.
- [33] Nuno Manuel Mendes Maia, Júlio Martins Monttalvão e Silva, Jimin He, Nicholas Andrew John Lieven, Rong Ming Lin, Graham William Skingle, Wai-Ming To, and António Paulo Urgueira. *Theoretical and Experimental Modal Analysis*. Engineering Dynamics Series. Research Studies Pres Ltd, Taunton, Sommerset, England, 1997.